

S. S. Matsyuk · K. Langer

Hydroxyl in olivines from mantle xenoliths in kimberlites of the Siberian platform

Received: 19 March 2003 / Accepted: 10 November 2003 / Published online: 26 February 2004
© Springer-Verlag 2004

Abstract From a total of 335 olivine crystal grains, crystallographically orientated platelets and, where possible, parallelepipeds were prepared, chemically analysed by electron microprobe, examined under the polarisation microscope, and studied by polarised FTIR microscope-absorption-spectrometry in the ν_{OH} vibrational range, 3,000–3,800 cm^{-1} . The 335 crystal grains were extracted from 174 different specimens of Yakutian upper mantle material, including 97 xenoliths that represent all the rock types occurring in all the kimberlites of the Siberian shield. The other specimens were mega- and macrocrysts or inclusions in diamonds and garnets. Analysis of the polarised ν_{OH} -spectra allowed for distinction between hydroxyl in non-intrinsic separate inclusions, NSI, and in isolated local or condensed extended defects, intrinsic to the olivines, ILD or CED, respectively. As the two latter types cannot be distinguished by vibrational spectroscopy, and as they are presumably interconnected by intracrystalline condensation reactions of the type $n [\text{ILD}] \rightleftharpoons [\text{CED}]_n$, we propose to symbolise them as $[\text{ILD}/\text{CED}]$. Of the total of 70 polarised ν_{OH} -bands that were found in the whole set, 17 are caused by NSI, 53 by $[\text{ILD}/\text{CED}]$. Total mean integrated ν_{OH} -band intensities, $\sum(\bar{\alpha}_{\text{int}})_{\text{total}}$ with $\bar{\alpha}_{\text{int}} = (\alpha_{\parallel a} + \alpha_{\parallel b} + \alpha_{\parallel c})_{\text{int}}/3$, were determined from the spectra. They yielded the contents of structurally unlocated “water”, using the recent calibration of the IR-method (Bell et al. 2003). The range is 0 < wt. ppm $(\text{H}_2\text{O})_{\text{total}} < 419$. Olivines included in diamonds were found to be free of hydroxyl (detection limit of the single crystal IR-spectrometry, ca. 1 wt. ppm “water”). The

total “water” contents of the different types of olivines increase in the sequence groundmass crystals < megacrysts < macrocrysts. NSI are: (1) Serpentine plus talc with ν_{OH} in the range 3,704–3,657 cm^{-1} , either polarised along **a** of the olivine matrix (*Pbnm* setting) or unpolarised. Approximately 232 olivines out of the 335 contain such NSI. Serpentine and talc occur mostly together, in rare cases one of them alone and if so, mostly talc. (2) Mg-edenite or Mg-pargasite occur rarely and with ν_{OH} at 3,709–3,711 cm^{-1} . NIS types (1) and (2) are presumably formed by metasomatic alterations of the host olivines, the orientated ones probably in the mantle, the unorientated ones during later stages. (3) The spectra of 23 olivine crystals, displayed specifically a ν_{OH} -band, polarised $c > a > b$, at 3,327–3,328 cm^{-1} , an energy typical of ν_{OH} in hydrous wadsleyite. We assume this phase to be present as NIS in the respective olivines, possibly as relic phase. (4) Weak bands between 3,175 and 3,260 cm^{-1} polarised along **c**, are tentatively assigned to molecular water NSI with relatively strong hydrogen bonds to the matrix. We did not find larger clusters of molecular water, i.e. liquid-like water with its characteristic broad band centred at ca. 3,400 cm^{-1} . We did also not find any humite minerals as an NSI. Of the 53 ν_{OH} -bands intrinsic to olivine, the 29 most abundant and strong ones were subject to further analysis in terms of OH^- -bearing structural defects $[\text{ILD}/\text{CED}]$. Nearly all these bands are strongly polarised along **a**. Two bands at 3,672 and 3,535 cm^{-1} are assigned to boron-related defects, $[\text{ILD}/\text{CED}]_{\text{B}}$. Five bands at 3,573, 3,563, 3,541, 3,524 and 3,512 cm^{-1} are intensity-correlated and are assigned to Si-depleted “titan-clinohumite-like” defects, $[\text{ILD}/\text{CED}]_{(\text{th})}$. The other, so far unidentified ν_{OH} of $[\text{ILD}/\text{CED}]$ are suggested to originate from OH^- in different types of (Mg, Fe)-depleted defects recently predicted and discovered by TEM. These are called $[\text{ILD}/\text{CED}]_{(\text{KWK})}$. Eight mostly strong bands of them occur at energies higher than 3,573 cm^{-1} , $[\text{ILD}/\text{CED}]_{(\text{KWK})-\text{H}}$, 13 strong to medium strong bands occur below 3,500 cm^{-1} , $[\text{ILD}/\text{CED}]_{(\text{KWK})-\text{L}}$. Such intrinsic defects may occur alone, $[\text{ILD}/\text{CED}]_{(\text{th})}$

Editorial responsibility: J. Hoefs

S. S. Matsyuk (✉) · K. Langer
Institute of Applied Geosciences, Technical University Berlin,
Ernst Reuter-Platz 1, 10623 Berlin, Germany
E-mail: ssmatsyuk@hotmail.com

S. S. Matsyuk
Institute of Geochemistry, Mineralogy and Ore Formation,
Ukrainian Academy of Sciences, Prospekt Palladina 34,
03142 Kyiv, Ukraine

and [ILD/CED]_{(KWK)-H}, or in different combinations with each other, [ILD/CED]_{(KWK)-H} + [ILD/CED]_(thl), [ILD/CED]_{(KWK)-H} + [ILD/CED]_{(KWK)-L} and [ILD/CED]_{(KWK)-H} + [ILD/CED]_(thl) + [ILD/CED]_{(KWK)-L}. Though there are indications that the occurrences of such types and combinations of the intrinsic OH⁻-bearing defects in the olivines are related to the types and genetic peculiarities of their host rocks, straightforward and simple correlations do not exist. The reasons for this and also for the great number of varieties of intrinsic [ILD/CED] are discussed.

Introduction

Since long, the occurrence of minerals with constitutive water-contents as phlogopite, titanclinohumite, edenite, pargasite in mantle rocks, and of fluid inclusions in mantle minerals formed the basis for an approach to an understanding of the role of water in mantle material.

During the last two decades, it became obvious—mostly from careful studies and evaluations of the valence vibrational region of hydroxyl-groups in the IR-spectra of single crystals of mantle minerals—that nominally “water”-free¹ mantle minerals may contain traces of “water” which are chemically bound in OH⁻-bearing intrinsic or non-intrinsic, zero- to three-dimensional structure defects. The analysis of such hydroxyl-defects in mantle minerals became a new possibility to approach the elucidation of the role of water in the mantle. Especially, two extended studies (Bell and Rossman 1992; Matsyuk et al. 1998) tried to explore the possible use of hydroxyl-bearing defects in an elucidation of genetic questions of mantle materials, on the basis of quantitative IR-spectroscopic determinations of the “water” contents in garnets of xenoliths in mantle kimberlites from below the South African and the Siberian shields. However, it is obvious from the two studies that the results of such work need completion by the study of the contents of hydroxyl-defects in other minerals typical of mantle rocks, in particular of olivines from a broad variety of different types of mantle rocks from different kimberlites.

Earlier work does not only prove the presence of hydroxyl-bearing defects in olivines of various origin (Beran 1969; Beran and Putnis 1983; Freund and Oberheuser 1986; Kitamura et al. 1987; Miller et al. 1987; Sykes et al. 1994; Libowitzky and Beran 1995; Kurosawa et al. 1997) but also forms the basis for quantitative evaluations of the “water”-contents in olivines (Paterson 1982; Bai and Kohlstedt 1992; Kohlstedt et al. 1996; Libowitzky and Rossman 1996, 1997; Bell et al. 2003). Also, various structural models of the incorporation of

hydroxyl and also of molecular water into the olivine structure have been proposed (Beran 1969; Beran and Putnis 1983; Kitamura et al. 1987; Libowitzky and Beran 1995; Kurosawa et al. 1997; De Leeuw et al. 2000; Kudoh 2002). Also, attempts were made to solve the involved questions by quantum mechanical calculations (Wright and Catlow 1994; De Leeuw et al. 2000). Experimental work on olivine (Bai and Kohlstedt 1992; Kohlstedt et al. 1996) was performed under thermodynamic conditions modelling mantle genesis of olivines, especially water and oxygen fugacities. The experiments were combined with IR-spectroscopic studies of the products to relate the occurrence of OH⁻-groups with the thermodynamic parameters. Such work may considerably contribute to an elucidation of the complicated O-H valence vibrational spectra of mantle olivines, as is also the case for TEM work on natural olivines in combination with IR-spectroscopy (Kitamura et al. 1987; Miller et al. 1987; Khisina et al. 2000, 2001; Khisina and Wirth 2002).

Despite all the just mentioned efforts, to elucidate the OH⁻ vibrational region 3,800–3,000 cm⁻¹ in the polarised IR-spectra of olivines, the problems of band assignment of such spectra is not solved so far. The difficulties are obvious when it is recalled that so far a total of 40 different mostly unassigned ν_{OH} -bands are identified in olivines of different origins. An exceptionally large number of ν_{OH} has been found in spectra of two olivines from the kimberlites of Monastery and Kimberley (Miller et al. 1987). This large number of OH⁻-bands in mantle olivines, studied so far, is unique among OH⁻-bearing defects in other nominally “water”-free minerals. Further, very small bandwidths, in the range of 4–20 cm⁻¹, and strict polarisations of most of the ν_{OH} -bands are characteristic of the OH⁻-bearing defects that may give rise to such bands in olivines (e.g. Beran and Putnis 1983; Libowitzky and Beran 1995).

In view of all the difficulties and ambiguities to which a straightforward assignment of the complex OH⁻-spectra of olivines and their quantitative evaluation in terms of intrinsic and non-intrinsic contents of the component “water” are currently still subject, the main tasks of the present paper are:

1. careful measurement, documentation and evaluation of polarised IR-spectra in the ν_{OH} -range, 3,800–3,000 cm⁻¹, on a large number of chemically and optically characterised olivine single crystals from a broad variety of different types of mantle rocks and associations from kimberlites of the Siberian platform,
2. wherever possible, identification of non-intrinsic ν_{OH} -bands originating from hydroxyl in material clearly to be classified as “inclusion”, and ν_{OH} -bands originating from defects intrinsic to the respective olivine or olivines,
3. check for correlations between band intensities of different bands on a quantitative basis. This seems promising when a large data basis of polarised spec-

¹Throughout the paper, we use the designation “water” for the structurally unspecified analytically determined total contents of the component water.

tra on a large number of olivine crystals is achieved under task (1),

4. check whether specific types of host xenoliths promote specific bands or band groups characterised as intrinsic or non-intrinsic,
5. determination of integrated intensities of the entire ν_{OH} -band envelope, $\sum(\bar{\alpha}_{\text{int},||a,b,c}) = \sum(1/t) \int (\log(I_0/D)_{||a,b,c}) \times dv$, to obtain quantitative information on total “water” contents using existing macroscopic calibrations (Bell et al. 2003). An attempt will be made to separate integrated intensities of non-intrinsic from intrinsic contributions to the evaluated total intensities $\sum(\bar{\alpha}_{\text{int},||a,b,c})$.

Material studied and experimental methods

Material studied

A total of 335 olivine single-crystal grains was extracted from a suite of 174 different mantle specimens, including 97 different xenoliths, representing all types of mantle rocks observed in Yakutian kimberlites, Siberia, as well as 25 olivine megacrysts and 49 olivine macrocrysts², two olivine crystals included in two diamonds and one olivine crystal included in a garnet megacryst. The extracted olivine single-crystal grains were studied by electron microprobe analysis and by polarised FTIR-microscope-spectrometry.

Wherever possible, the mantle xenoliths were selected under the following viewpoints:

1. samples of the same rock-type, e.g. dunites, harzburgites, lherzolites etc., formed under the conditions of either the diamond-pyrope, the graphite-pyrope or the spinel-pyroxene facies (Sobolev et al. 1972) should be available,
2. mantle rocks, mega- and macrocrysts, from the three just mentioned facies should be available from a series of different kimberlites between the centre (e.g. Mir, Udachnaya) and the north (Obnazhonaya, Slyudyanka, etc.) of the Siberian platform.

Results on 65 olivine crystals (Table 1, column 6) obtained from a total of 34 different mantle specimens (Table 1, column 1), typical for the whole set of 174 mantle specimens, were selected for the detailed presentation in the present paper. The olivine crystals were extracted from 19 different xenoliths, from one diamond or from one garnet megacryst; 8 were olivine megacrysts and 5 macrocrysts. Aside the samples, Table 1 compiles the kimberlite localities, the mantle-facies (Sobolev et al. 1972) and the rock types that contain the respective olivine. Quoted are also the crystal plates, prepared for the measurements, as well as their thicknesses. The samples are grouped in Table 1 according to the rock

series to which they belong. Such genetically different rock series were proposed for a systematic description by Matsyuk et al. (1988) and Platonov et al. (1988). They are illustrated and their interrelations are shown by Matsyuk et al. (1998, Fig. 1).

Experimental methods

Preparation of crystal plates

At least two crystal fragments from each mantle specimen were selected for preparation as crystallographically differently orientated platelets, mostly (010) and (001), in some cases also (100). On these, polarised spectra with $E||a(||Z)$, $E||b(||X)$ and $E||c(||Y)$ could be obtained. The orientations given here refer to the most widely used space group setting *Pbnm* of the olivine structure (Bragg and Brown 1926). The related orientations of the axes of the optical indicatrix, $X(n_x)$, $Y(n_y)$ and $Z(n_z)$, are given according to Tröger (1971). Olivine crystals from some of the rock samples, especially from cataclastic porphyritic and from cataclastic porphyritic-like nodules, turned out to be inhomogeneous with respect of the spectra obtained. In such cases, a total of four to six crystal plates of the same orientation have been prepared and measured. Some olivine crystals (26) were prepared as orientated parallelepipeds, allowing for measurements in all three polarisations on one and the same crystal.

The preparational steps to obtain the plates or the parallelepipeds polished on the faces to be penetrated by the measuring radiation, were described previously (Matsyuk et al. 1998). The orientations of all plates and the parallelepipeds were controlled and checked by microscopic methods. Deviations from the exact orientations $||\{010\}$, $||\{001\}$ or $||\{100\}$ do not exceed 1–2° for the majority of the crystal plates, and 3–5° for very few ones only.

All crystal plates and parallelepipeds prepared were carefully examined under the polarising microscope as it was also done for thin sections of the host rock samples. Most of the prepared specimens were clear or contained at least optically clear parts large enough to allow for the IR-microscope-spectrometric measurements.

Electron microprobe analyses

The chemical compositions of the olivine crystals studied were obtained by electron microprobe analyses using instruments and methods of measurement, standardisation and evaluation as described before (Matsyuk et al. 1998). Microprobe analyses were taken at several spots on the crystal under study, including spots inside the selected measuring areas of the IR-spectroscopy. Trace element analyses, especially of boron and lithium could not be obtained on the large set of samples. This might be counted a deficit of this study because trace elements influence the local potential fields in which the OH^- -groups intrinsic to the respective olivine, vibrate. However, such effects bear on the elucidation of the structural allocation of intrinsic “water”. As stated before, structural allocation of intrinsic OH^- -groups is not a necessary condition for our quantitative task.

Polarised IR-microscope-spectrometry

Polarised single-crystal IR-spectra, were measured in the spectral range 3,800–3,000 cm^{-1} , where OH^- -valence vibrations are known to occur in olivines (cf. introduction). The FTIR-spectrometer (Bruker ISS 66) equipped with an IR-microscope, as well as the methods of measurement were the same as in Matsyuk et al. (1998). The instrument was operated at a spectral resolution of 1 cm^{-1} , the measuring spot had a diameter of 100 μm . Linear polarisation of the measuring radiation close to 100% is required for reliable

²Here, megacrysts or macrocrysts are defined as those crystals with smallest dimension larger than 1 cm or ~0.5–1 cm, respectively.

Table 1 Olivine crystals studied: Olivines from mantle-rocks, olivine megacrysts, olivine macrocrysts and olivine inclusions in diamond and garnet from kimberlites of the Siberian platform, Yakutia. Abbreviations in the second column designate the kimberlite type from which the nodules were collected: *M*Mir, *U* Udachnaya, *O* Obnazhonnaya, *SL* Slyudyanka, *WT* Wtorogodniza, *K* Kiyevlyanka, *CH* Chorey, *B-3* Bazovaya-3. *M* occurs in the Malo-Botuobinskoye kimberlite field; *O*, *SL*, *WT*, *K*, and *CH* in the Kuoyksko-Beenchimskoye field and *B-3* in the Charamaiskoye field. Abbreviations characterising the host rock facies (Sobolev et al. 1972): *D-Py* diamond-pyroxene facies, *G-Py* graphite-pyroxene facies, *Sp-Px* spinel-pyroxene facies. *Uv-406* collection and analysis Sobolev et al. (1984). The third column refers to the rock series to which the respective samples belong, according to the nomenclature also used by Matsyuk et al. (1998). Textural characteristics are abbreviated as *cg* coarse grained, *cp* cataclastic porphyritic (garnet blasts > 2 mm), *cpl* cataclastic porphyritic-like (garnet blasts ≈ 0.5–1.5 mm). For abbreviations of mineral phases: *D* diamond, *Gt* garnet, *Ol* olivine, *Ol_g* recrystallised olivine from the ground mass, *Ol_r*, relic olivine, *Cpx* clinopyroxene, *Sp* spinel, *Ilm* ilmenite. Asterisks mark samples, where coexisting garnets have also been studied (Matsyuk et al. 1998); *t* plate thickness

Sample no.	Locality	Rock series	Rock facies	Rock (and association)	Prepared crystals		Orientation	t, mm	Characteristics
					Crystal no.	Orientation			
A-176	M	Mg	D-Py	Gt-harzburgite, cg	K1	(010)	0.284	Colorless, clear (cl)	
Tw-176/79	U			Gt-harzburgite, cg	K2	(001)	0.352	Colorless, faint yellow hue, cl	
					K1	(010)	0.302		
Tw-9/79*	U			Gt-harzburgite, cg	K2	(001)	0.316	Light yellowish green, cl	
					K1	(010)	0.590		
A-47	M		G-Py	Gt-lherzolite, cg	K2	(001)	0.255	Colorless cl	
					K1	(010)	0.402		
O-89*	O			Sp-Gt-lherzolite, cg	K2	(010)	0.271	As A-176	
					K1	(010)	0.355		
O-8	O			Garnetized lherzolite, cg	K2	(001)	0.476	Colorless with light green hue, cl	
					K1	(010)	0.488		
Ps-92/84	B-3		Sp-Px	Sp-harzburgite, cg	K2	(001)	0.332	As O-8	
					K1	(010)	0.492		
C-2/9	U	Mg-Ca	D-Py	Inclusion in diamond	K2	(001)	0.428	As A-176	
					K1	(010)	0.113		
Uv-406	U			D-bearing Gt-dumite	K1	(010)	0.478	As O-8	
					K2	(001)	0.338		
Twd-40a/77	U			Gt-dumite, cg	K1	(010)	0.661	As O-8	
					K2	(001)	0.883		
Twd-20*	U			Ol-megacryst with included Gt and Sp	K1	(010)	0.585	Slightly yellowish green, cl	
					K2	(001)	0.608		
Twd-29	U			Ol-megacryst with included Gt	K1	(010)	0.564	Slightly olive green, cl	
					K2	(001)	0.526		
A-5	M			Gt-harzburgite, cg	K1	(010)	0.548	Slightly greenish yellow, cl	
					K2	(001)	0.502		
A-379	M			Gt-harzburgite (Cpx = 3%), cg	K1	(010)	0.436	Light greyish yellow, cl	
					K2	(001)	0.436		
Tw-250/79	U		G-Py	Gt-harzburgite, cpl	Ol _g	(010)	0.493	As A-5	
					Ol _r	(001)	0.505		
							0.629	Slightly brownish yellow, cl	
							0.518		

Table 1 (Contd.)

Sample no.	Locality	Rock series	Rock facies	Rock (and association)	Prepared crystals			Characteristics
					Crystal no.	Orientation	t, mm	
Tw-281/79	U			Gt-wherlite, cg	K1 K2	(010) (001)	0.362 0.372	Light yellow green hue, cl As Twd-20
Tw-48/79	U			Gt-lherzolite, cpl	Ol _g	(010)	0.260	
						(001)	0.226	Slightly brownish yellow, cl As Twd-20, deformation lamellae (100), cl
Twd-24	U			Ol-megacryst	Ol _r	(010) (001)	0.455 0.321	
					K1 K2	(010)	0.542	Olive green, turbid, deformation lamellae (100), cl
Wt-23/87	WT			Ol-megacryst	K1	(001)	0.582	
						(010)	4.212	Olive green, faint turbidity As Twd-20
K-4	K			Ol-megacryst	K1	(001)	3.320	
					K2	(010)	0.742	Olive green, turbid, deformation lamellae in various orientations
Ud-118	U			Ol-macrocryst	K1	(001)	0.374	
						(010)	2.852	Light olive green, slightly turbid As F-38, polysynthetically twinned As Twd-20
						(001)	2.136	
F-38	U			Ol-phenocryst	K1	(010)	0.380	Light olive green, slightly turbid As F-38, polysynthetically twinned As Twd-20
F-67 g	U			Ol-phenocryst	K1	(001)	0.568 0.748 0.537	
						(010)	0.492	Light yellowish brown, cl
Twd-39	U	Ca	G-Py	Ol-megacryst with included Gt (CaO = 8.7%, Cr ₂ O ₃ = 4.0%) Ilm-Gt-wherlite, cp	K1 K2	(010) (001)	0.382	
						(010)	0.300	Light yellowish brown, cl
Tw-194/77	U	Mg-Fe	G-Py		K1 K2	(010) (001)	0.538	
						(010)	0.295	Light yellow, cl
Sl-278	SL			Ilm-Gt-lherzolite, cg	K1 K2	(010) (001)	0.235	
						(010)	0.372	As Tw-194/77, deformation lamellae (100)
X-8	CH			Ol-megacryst	K1 K2	(010) (001)	0.425	
						(010)	2.970	Yellowish brown, cl
Wt-47/87	WT			Ol-megacryst	K1 K2	(010) (001)	0.662	
						(010)	0.200	As Tw-194/77
Tw-216/79	U			Gt-megacryst with included olivine	K1 K2	(010) (001)	0.198	
						(010)	0.447	As F-38
F-44	U			Ol-macrocryst	K1	(001)	0.348	

Table 1 (Contd.)

Sample no.	Locality	Rock series	Rock facies	Rock (and association)	Prepared crystals		t, mm	Characteristics
					Crystal no.	Orientation		
F-68	U			Ol-macrocryst	K1	(010) (001)	0.430 0.417	Slightly brownish yellow, cl Light brown, cl
SI-98	SL		Sp-Px	Ilm-dunite, cg	K1 K2	(010) (001)	0.520 0.328	Colorless with faint yellow hue, cl
SI-387	SL			Ilm-Ti-clinohumit-dunite with K-richterite, cg	K1 K2	(010) (001)	0.221 0.402	As Tw-194/77
O-80/87	O			Ilm-lherzolite, cg	K1 K2	(010) (001)	0.451 0.455	

quantitative evaluation of the polarised spectra obtained (Libowitzky and Rossman 1996). The polariser of the IR-microscope used here, showed—if any—only a very small fraction of unpolarised radiation in the spectral range of the measurements. This is obvious from polarised measurements of the ν_{OH} -range of amphiboles (M. N. Taran, personal communication) the spectra of which are known from the literature.

Generally, spectra were scanned at room temperature. Some selected crystals were also studied at 100 K using a Linkam cooling table and liquid N₂, the platelets being held on a gold wire grid. For most specimens, two crystal plates, e.g. a (010)- and a (001) plate, have been prepared from different olivine crystals (cf. Table 1). Such plates allow for the measurement of one of the three polarisations in both plates, in the example E||a. Only those spectra E||a, b and c were combined in the figures to be shown and discussed, where the spectra of the same orientation recorded on the two plates had the same shape, especially same band intensities. For Tw-250/79 and Tw-48/79, relic as well as ground mass (recrystallised) olivines were prepared (Table 1) and measured. The spectra presented here, were recorded on the recrystallised olivines. All the spectra shown in the present paper are unmanipulated “raw” spectra, except for recalculating the ordinate values to $\alpha = \log(I_0/I)/t$, with t = measured plate thickness in cm.

Curve resolution of the mostly very complex spectral envelopes was achieved by the same methods already used for garnet spectra (Matsyuk et al. 1998). Straight lines between the α values at 3,000 and 4,000 cm⁻¹ (cf. Fig. 1) served as base lines. Only such analysed component bands were considered as true ones that were discernible as maxima, inflections or shoulders by means of by-eye-inspection of the spectrum just analysed. Only in those spectral regions where the observed and calculated total spectral envelopes deviated unacceptably from each other, an additional band was introduced. Data from analysed spectra used in tables, figures or in the text, are band positions³, (wavenumber) ν in [cm⁻¹], bandwidths (full width at half band height), $\Delta\nu_{1/2}$ in [cm⁻¹], and band intensities in terms of linear absorption coefficients, $\alpha_{lin} = \log(I_0/I)/t$ in [cm⁻¹] as well as integral absorption coefficients, $\alpha_{int} = (1/t) \int \log(I_0/I) \times d\nu$ in [cm⁻²]. Total integrated intensities are given as mean values, $\sum(\bar{\alpha}_{int}) = (\alpha_{|X} + \alpha_{|Y} + \alpha_{|Z})_{int}/3$ (cf. Maldener et al. 2003) and were subject to estimated errors of $\pm 5\%$. The thicknesses used to normalise the integrated absorbencies, $\int \log(I_0/I) d\nu$, to a plate thickness of 1 cm, are the uncorrected t-values as quoted in Table 1. Maldener et al. (2003) showed that such thicknesses may deviate in microscope-spectrometric measurements from the effective ones by the convergence of the measuring beam. However, for a beam diameter of 100 μ m used here, such effects do not exceed 5%. In addition, measurements of the same orientation on crystals with different measured thicknesses yielded spectra with the same $\sum(\bar{\alpha}_{int})$ -values within the experimental error.

Results, their evaluation and discussion

Experimental results

The chemical compositions of olivine crystal plates (Table 1), were recalculated from the results of electron microprobe analyses to atoms per formula unit and are presented in Table 2. The data show that the olivines selected here, represent almost the whole range of chemical variation from 6.5 to 18.2 mol% fayalite end member, known for mantle olivines from Yakutian kimberlites (Ukhanov et al. 1988; Matsyuk and Zintchouk 2001).

³Energies of clearly discernible band maxima were determined by inspection of several spectra of the same crystal plate.

Table 2 Results of electron microprobe analyses of olivines extracted from the mantle specimens listed in Table 1. The data are presented as atoms per formula unit. The uncertainty is in the last decimal point. *n.a.* not analysed

Olivine from	At. pfu										Σ
	Mg	Fe ²⁺	Mn	Ca	Co	Ni	Al	Cr	Ti	Si	
A-176	1.852	0.148	0.0018	0.0000	0.0006	0.0069	0.0000	0.0000	0.0000	0.996	3.005
Tw-176/79	1.852	0.144	0.0023	0.0016	n.a.	n.a.	0.0003	0.0002	0.0000	1.000	3.000
Tw-9/79	1.846	0.147	0.0014	0.0005	0.0010	0.0079	0.0000	0.0004	0.0000	0.998	3.002
A-47	1.840	0.166	0.0012	0.0000	n.a.	n.a.	0.0000	0.0000	0.0002	0.996	3.005
O-89	1.853	0.149	0.0010	0.0003	0.0000	0.0071	0.0003	0.0000	0.0007	0.994	3.005
O-8	1.873	0.129	0.0018	0.0003	0.0004	0.0078	0.0006	0.0000	0.0009	0.993	3.007
Ps-92/84	1.857	0.148	0.0018	0.0005	0.0000	0.0077	0.0009	0.0008	0.0005	0.991	3.008
C-2/9	1.860	0.132	0.0000	0.0003	0.0004	0.0074	0.0000	0.0008	0.0000	1.000	3.001
Uv-406	1.867	0.134	0.0012	0.0003	0.0000	0.0069	0.0003	0.0008	0.0002	0.995	3.006
Tw-40a/77	1.852	0.145	0.0014	0.0008	0.0004	0.0067	0.0003	0.0002	0.0004	0.996	3.003
Tw-20	1.858	0.139	0.0004	0.0005	n.a.	n.a.	0.0000	0.0004	0.0004	1.000	2.999
Tw-29	1.816	0.166	0.0004	0.0003	0.0006	0.0076	0.0000	0.0002	0.0002	1.004	2.995
A-5	1.858	0.142	0.0020	0.0003	0.0004	0.0065	0.0006	0.0009	0.0002	0.994	3.005
A-379	1.854	0.148	0.0018	0.0000	0.0004	0.0050	0.0003	0.0006	0.0002	0.995	3.005
Tw-250/79	1.837	0.149	0.0025	0.0005	n.a.	n.a.	0.0000	0.0006	0.0008	1.004	2.994
Tw-281/79	1.832	0.173	0.0012	0.0010	0.0002	0.0066	0.0006	0.0000	0.0009	0.992	3.008
Tw-48/79	1.781	0.184	0.0035	0.0021	0.0000	0.0073	0.0000	0.0021	0.0007	1.009	2.990
Tw-24	1.786	0.217	0.0025	0.0003	n.a.	n.a.	0.0009	0.0000	0.0002	0.996	3.003
Wt-23/87	1.834	0.164	0.0019	0.0008	n.a.	n.a.	0.0015	0.0010	0.0006	0.997	3.001
K-4	1.838	0.163	0.0023	0.0011	n.a.	n.a.	0.0000	0.0016	0.0004	0.996	3.002
Ud-118	1.822	0.165	0.0033	0.0010	0.0013	0.0050	0.0003	0.0006	0.0009	1.000	2.999
F-38	1.863	0.140	0.0022	0.0003	0.0000	0.0075	0.0000	0.0013	0.0000	0.993	3.007
F-67 g	1.823	0.174	0.0018	0.0008	0.0006	0.0068	0.0014	0.0021	0.0002	0.994	3.005
Tw-39	1.856	0.129	0.0035	0.0008	n.a.	n.a.	0.0006	0.0004	0.0004	1.004	2.995
Tw-194/77	1.740	0.250	0.0027	0.0005	0.0004	0.0055	0.0003	0.0004	0.0004	1.000	3.000
Sl-278	1.723	0.274	0.0030	0.0008	n.a.	n.a.	0.0003	0.0002	0.0004	0.999	3.001
X-8	1.661	0.335	0.0028	0.0008	n.a.	n.a.	0.0018	0.0000	0.0011	0.998	3.001
Wt-47/87	1.775	0.229	0.0038	0.0005	0.0006	0.0050	0.0000	0.0004	0.0006	0.992	3.007
Tw-216/79	1.732	0.252	0.0021	0.0022	n.a.	n.a.	0.0003	0.0002	0.0002	1.006	2.995
F-44	1.804	0.195	0.0020	0.0021	0.0006	0.0077	0.0008	0.0009	0.0007	0.992	3.006
F-68	1.773	0.225	0.0025	0.0010	0.0006	0.0063	0.0009	0.0008	0.0005	0.994	3.005
Sl-98	1.620	0.363	0.0030	0.0022	0.0008	0.0012	0.0012	0.0002	0.0011	1.003	2.996
Sl-387	1.788	0.210	0.0059	0.0005	0.0004	0.0056	0.0003	0.0000	0.0000	0.995	3.006
O-80/87	1.671	0.307	0.0015	0.0011	0.0008	0.0046	0.0018	0.0008	0.0002	1.005	2.994

Selected typical spectra at ambient conditions, in the ν_{OH} -range for the polarisations $\mathbf{E}||\mathbf{a}(\parallel\mathbf{Z})$, $\mathbf{E}||\mathbf{b}(\parallel\mathbf{X})$ and $\mathbf{E}||\mathbf{c}(\parallel\mathbf{Y})$ of olivines are displayed in Fig. 1a, b. The spectra which were not included in this figure for clarity, are very close to the included ones and will be commented later. Energies of the total of 70 bands observed in the olivines (Tables 1 and 2) are compiled in Table 3 together with their polarisations. Figure 1 displays complex band envelopes. To make the recognition of occurrences and positions of bands easier, faint lines are drawn in Fig. 1 and are labelled by the band numbers of Table 3. For comparison, this table lists also the bands found by Libowitzky and Beran (1995) in polarised spectra of a near-to-end-member forsterite from Tadshikistan, and by Miller et al. (1987) in an olivine from a xenolith in the kimberlite at Monastery, Winbury/S.A. It is obvious that all bands observed by these authors are present also in the total of our spectra.

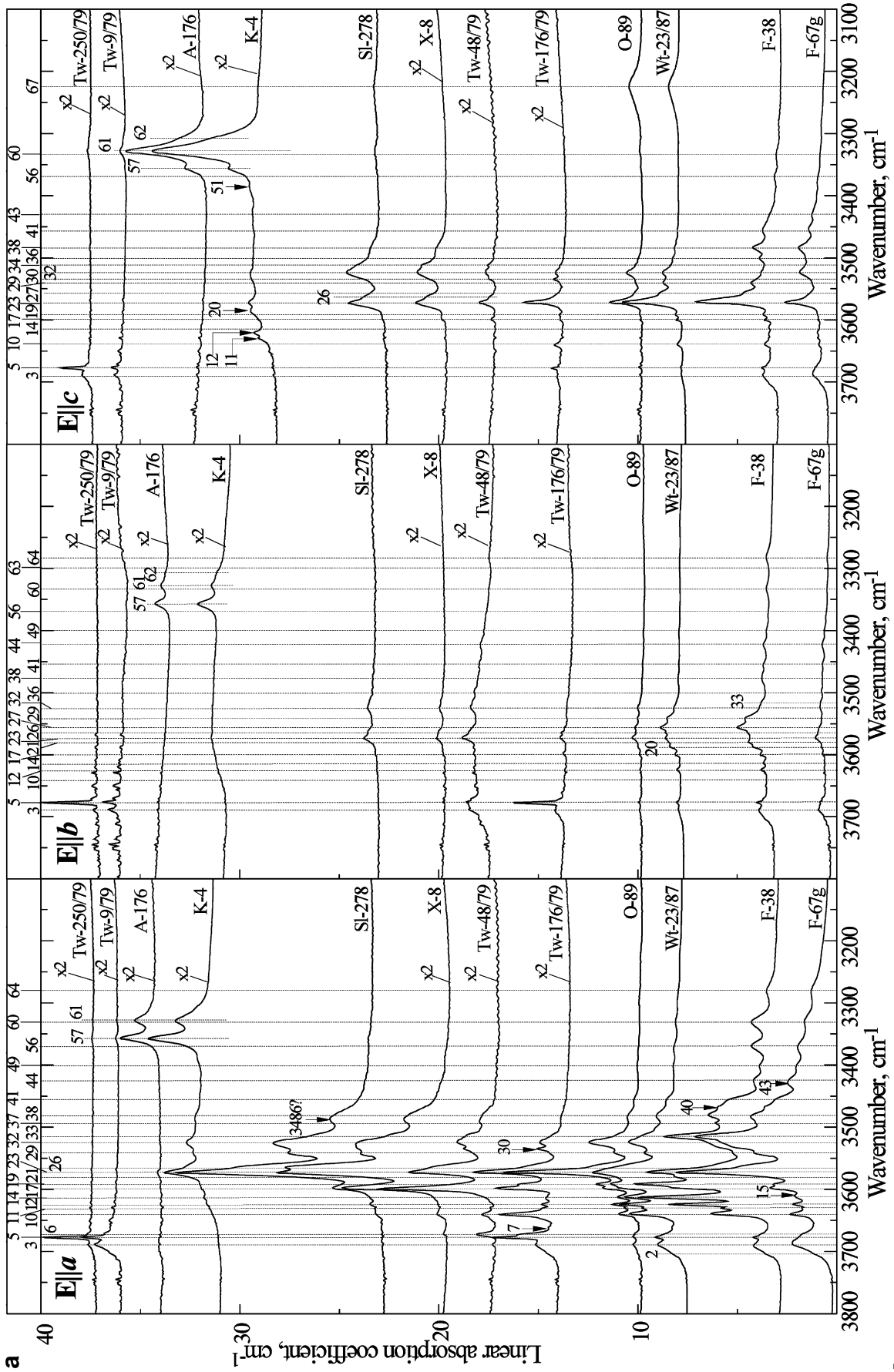
All bands showing up as discrete peaks or shoulders, sometimes faint shoulders, in the spectra measured in this study are true features of the respective crystal, as all of them are reproduced in repeated spectral recordings. The complex patterns of ν_{OH} -bands are not caused or caused in part by hydroxyl in the surface layers of the plates which

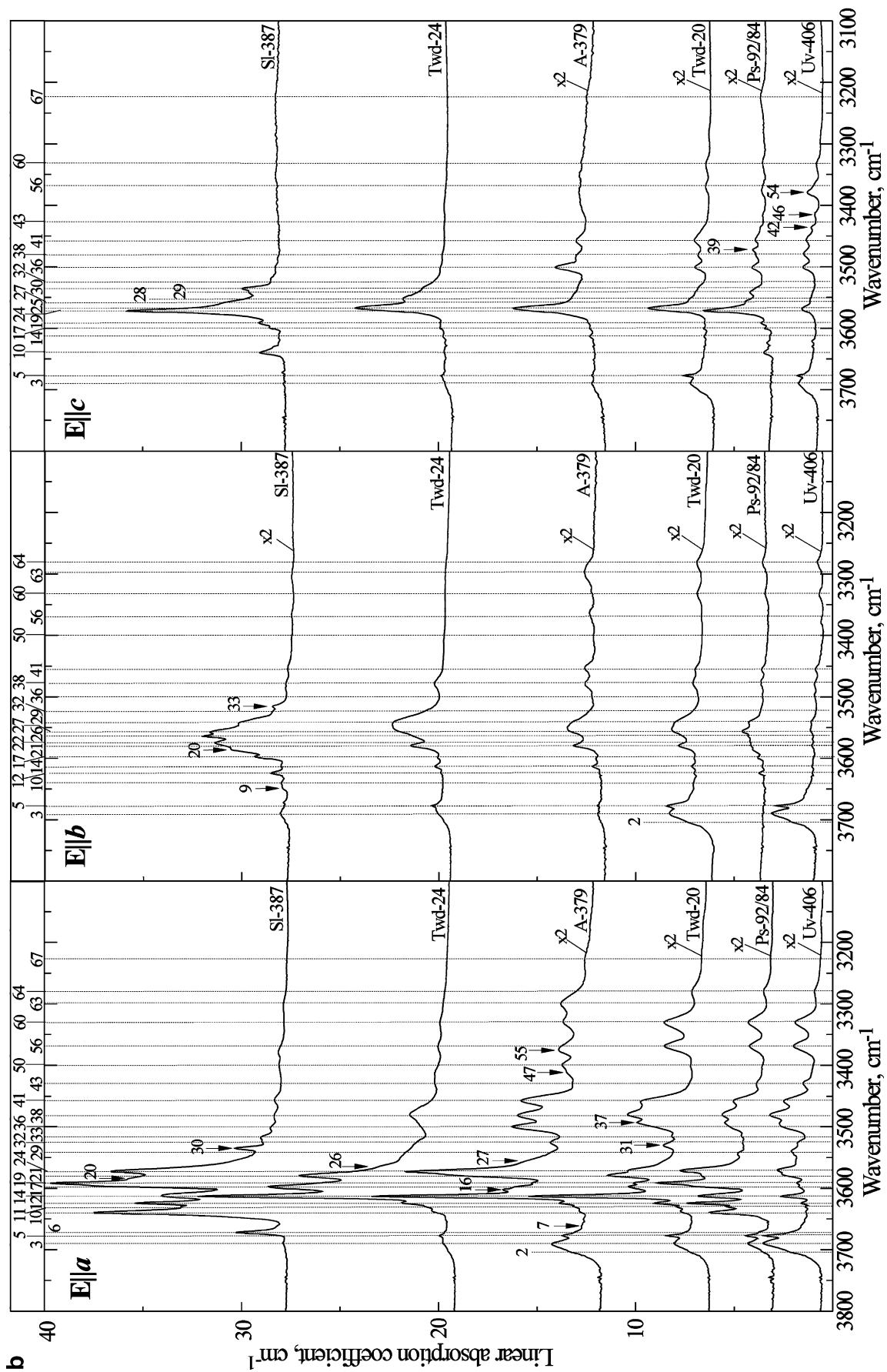
are disturbed by polishing, the so-called Beilby-layers (Beilby 1921; Bowden and Hughes 1937a, 1937b). This is obvious from the fact that in NRA-profiles, Beilby layers on olivines are found to be about 0.2 μm thick (see Bell et al. 2003). Hence, the total thickness of the disturbed surface, ca. 0.4 μm , amounts at maximum 0.4% of the total thickness of the thinnest plate measured here (113 μm , sample C-2/9 in Table 1).

Bandwidths are very small, in the range of 2 to 20 cm^{-1} at energies down to 3,500 cm^{-1} , and grow increasingly broader, up to 40 cm^{-1} , on further decreasing energy down to 3,200 cm^{-1} . Most of the bands are polarised parallel to $\mathbf{a}(\parallel\mathbf{Z}, n_{\gamma})$, in fact a great number of them strictly parallel to \mathbf{a} . This is in accor-



Fig. 1 Main types of OH^- -valence vibrational spectra observed in the present paper on the mantle olivines studied. The spectra are scanned at 298 K with polarised radiation, on the platelets listed in Table 1. The numbers on top of the two parts of the figure are the band numbers used in Table 3. Spectra characterised by $\times 2$ are enlarged with respect of the ordinate by a factor of 2. Sample numbers characterising the spectra are those of Table 1. Except for thickness normalisation, $\log(I_0/I)/t$, the spectra are uncorrected. For clarity, the spectra are ordinate shifted, the background of all the spectra at 3,800 cm^{-1} is very close to $\log(I_0/I)/t = 0.5 \text{ cm}^{-1}$





dance with earlier results of Beran and Putnis (1983), Miller et al. (1987) and Libowitzky and Beran (1995). Some of the bands have high intensity in $\mathbf{E}||\mathbf{c}(\parallel\mathbf{Y}, n_\beta)$, few ones in $\mathbf{E}||\mathbf{b}(\parallel\mathbf{X}, n_\alpha)$ (Fig. 1, Table 3).

From inspection of the three complex ν_{OH} -spectra, $\parallel\mathbf{a}$, $\parallel\mathbf{b}$, and $\parallel\mathbf{c}$ of a specific olivine in Fig. 1, it is obvious that they result from combinations and superpositions of different bands and/or band groups from the total of 70 absorptions of Table 3. This statement seems to be trivial, but allows in combination with the information in Table 1 on localities and rock types, for the first qualitative conclusions:

- (c.1) Olivines from different “geological milieus” and/or with different history contain different types of OH^- -bearing defects, be they intrinsic or non-intrinsic, and possibly also water, be it molecular H_2O or clustered $(\text{H}_2\text{O})_n$.
- (c.2) Olivine C-2/9 extracted from a diamond, does not contain hydroxyl, at least not above the detection limit of the single crystal IR-spectroscopy (about 1 wt. ppm “water”, see above).

Evaluation and discussion

General considerations

It might be suspected that ν_{OH} of other “water”-bearing phases occurring as inclusions in the respective olivine host crystal contribute to the very rich variety of different ν_{OH} -bands observed in olivines. Therefore, it is necessary to differentiate between intrinsic and non-intrinsic ν_{OH} -bands. The first are those typical of hydroxyl on oxygen positions in the olivine structural matrix itself, including submicroscopic modifications of the structure by isolated local or by clustered defects, the latter forming extended structural modifications. In the following, the isolated local defects will be abbreviated as ILD, the clustered defects that form extended structure modifications as CED. On the other hand, non-intrinsic ν_{OH} -bands are those that originate from separate inclusions of other “water”-bearing minerals. These will be called NSI in the following.

To differentiate between intrinsic and non-intrinsic ν_{OH} , we follow here the reasoning of Miller et al. (1987, p. 467). In short, these authors argue as follows:

- (a) If some of the ν_{OH} observed in olivine spectra, coincide completely in energy, bandwidth and, eventually in the intensity ratio or ratios of the respective ν_{OH} , with those of an isolated large-sized mineral, as e.g. serpentine, then such ν_{OH} should be assigned to the respective mineral phase occurring as inclusion in olivine, i.e. these ν_{OH} is/are non-intrinsic (NSI).
- (b) “Conversely, if no common associated hydrous phase corresponds to an OH band, that band is considered intrinsic to olivine as a modification of its structure”. (ILD and CED in our terminology).

- (c) In the course of their argumentation, Miller et al. (1987) mention also the possibility that “If on the other hand, only a few unit cells of the hydrous phase were present in the olivine crystal, then the OH^- -absorption of the hydrous phase might be shifted in position and its width ...”. This is a special case of what is called above “clustered defects ... forming extended structural modifications” (CED). OH^- -vibrations from two- or three- dimensional clustered defects, CED, should definitely be regarded intrinsic, as was done above in the case of ILD.

In recent studies of two mantle olivine crystals from nodules #105 and #9206 of the Udachnaya kimberlite, Yakutia by TEM methods, Khisina et al. (2001) and Khisina and Wirth (2002) discovered three types of hydroxyl bearing “units” in the studied spots of the crystals: “large” inclusions of hydrous magnesium silicates such as serpentine, talc and 10 Å-phase that can be regarded as NSI. Further, the above authors found clustered defects, CED in our terminology. These occur as 20 to 50 nm thick lamellae and as very small spots with sizes up to several 10 nm. The latter are linked to dislocations in olivine from #9206 and to the lamellar defects in that from #105. Both types of CED were found to be (Mg, Fe)-depleted compared to the olivine matrix, Si contents are about the same. The larger lamellar CED are structurally coherent to olivine and are identified as “hydrous” olivine with composition $(\text{Mg}_{1-y}\text{Fe}^{2+}_y)_{2-x}\text{V}_x\text{SiO}_4\text{H}_{2x}$ (Khisina and Wirth 2002), as predicted on the basis of crystal chemical considerations, by Kudoh (2002). The volume fraction of the CEDs does not exceed 0.1 to 0.2% (R. Wirth, personal communication 2002). Khisina and Wirth (2002) conclude that “From the observations, it is obvious that the “hydrous” olivine (CED in our terminology) was precipitated from the olivine matrix, which initially was saturated in OH point defects (ILDs in our terminology), by an exsolution process” and that this process occurs at mantle conditions.

The ILDs have sizes in the atomistic scale and are, thus, not seen by TEM. It is suggested that they are of the type $[\text{V}_{(\text{Mg,Fe})}^{2-} + 2(\text{OH}^-)_{\text{O}2-}]$ (R. Wirth, personal communication, 2002). Because the volume fraction of the CEDs is very small, it is likely that they coexist with still present, uncondensed ILDs of the just mentioned type. Other ILDs in olivine are possibly $[\text{V}_{\text{Si}4-} + 4(\text{OH}^-)_{\text{O}2-}]$, as suggested by Beran and Putnis (1983) and Libowitzky and Beran (1995) to explain the observed polarisation behaviour of the ν_{OH} bands in the olivines they studied (cf. legend of Table 3).

To sum up this discussion, the complex set of ν_{OH} bands observed in the large variety of olivines of the present study (Table 3) is caused by three main groups of hydroxyl bearing “volume elements” in the olivine crystals: different types of non-intrinsic NSI’s; of intrinsic CEDs, possibly also different types; and finally, of different types of intrinsic ILDs, where the ILDs and CEDs are likely related to the state of primary “water”-

Table 3 All bands with their energies and polarisations, observed in the polarised olivine spectra of the whole suite of 174 specimens, and their comparison with the bands observed by Libowitzky and Beran (1995) on a near to end-member forsterite from Pamir/Tadzikistan and by Miller et al. (1987) on an olivine in a xenolith from the Monastery Farm, Winburg/S.A. Wavenumbers printed in italics characterise bands observed by Miller et al. (1987) in olivines from other localities than Monastery. Band pleochroism is schematically presented in column 7. The basis for determining the

pleochroism were the α_{lin} -values as obtained from curve resolution of the polarised spectra of 28 parallelepipeds of different olivines. Their spectra represent the whole set of bands listed in the Table. Column 8 characterises bands originating from included phases producing non-intrinsic bands, NSI (cf. text). Abbreviations: *TT* observed only at low temperature, *w* weak, *vw* very weak, *b* broad. Abbreviations in column 8: *A* amphibole, *MW* molecular water, *S* serpentine, *T* talc, *W* wadsleyite. *n* number of specimens which show the respective band

Band no.	Libowitzky and Beran (1995)	Miller et al.(1987)	v, cm ⁻¹			Pleochroism	NSI	n
			a	b	c			
1			3,709–3,711	3,709–3,711	3,709–3,711	–	A	6
2		<i>3,709</i>	3,704	3,704	3,704	–	S	> 100
3			3,688–3,692	3,688–3,692	3,688–3,692	–	S	> 100
4		<i>3,685</i>	3,684	3,684	3,683–3,684	–	L	> 20
5		<i>3,678</i>	3,677	3,677	3,677	–	T	> 100
6	3,674A		3,672	3,672	3,672	<i>a > c > b</i>		> 10
7			3,661–3,662	3,661–3,662w	3,662w	–	T	> 20
8		<i>3,657</i>	vw	vw	vw	<i>a ≈ b ≈ c</i>	S	> 10
9	3,647B	<i>3,645</i>	3,648–3,651w	3,649–3,650w	vw	<i>a > b ≥ c</i>		> 10
10	3,640C	3,637	3,639–3,640	vw	3,639w	<i>a > > c > b</i>		> 50
11			3,629–3,630	3,629	3,629	<i>a > c > b</i>		> 50
12	3,624D	3,623	3,624	w		<i>a > > b > c</i>		> 50
13			3,620w	3,620vw	3,620w	<i>c > a > b</i>		4
14		<i>3,612</i>	3,613	w	vw	<i>a > > b > c</i>		> 50
15		TT	3,608–3,609w			<i>a > b ≥ c</i>		2
16		<i>3,602</i>	3,602w			<i>a > c ≈ b</i>		6
17	3,598E	3,598	3,599	3,599–3,600w	3,599–3,600w	<i>a > > c ≥ b</i>		4
18			3,597	3,597–3,598w	3,597–3,598w	<i>a > > c ≥ b</i>		> 100
19	3,592F	3,591	3,591–(3,592)		3,591w	<i>a > > c > b</i>		> 100
20			3,584–(3,585)	3,586–3,587	vw	<i>a > b > c</i>		2
21			3,578–(3,579)	3,579	vw	<i>a > > b > c</i>		> 50
22			3,575	3,575		<i>a > b > > c</i>		1
23		<i>3,573</i>	3,573	3,573	3,573	<i>a > > c > b</i>		> 120
24	3,570G		3,570–(3,572)	vw	3,570–(3,572)	<i>a > c > > b</i>		> 20
25		<i>3,567</i>	w	vw	3,566–(3,570)	<i>c > a > > b</i>		> 10
26		3,562	3,562–3,564	3,562–3,564	3,562–3,563	<i>a > > c > b</i>		> 120
27			w	3,555–3,557	3,555–3,556	<i>b ≥ c ≥ a</i>		> 10
28			3,550	3,550–3,552	3,552	<i>c ≥ b ≥ a</i>		5
29		<i>3,541</i>	(3,538)–3,541	3,541	3,541vw	<i>a ≥ b ≥ c</i>		> 120
30	3,535H		3,535	vw	3,535	<i>a > c > b</i>		> 10
31			3,530			a		5
32	3,524I	3,524	3,524–(3,525)	3,525w	3,524–(3,525)	<i>a > c > b</i>		> 120
33	3,514J		3,515	3,515w	vw	<i>a > b > c</i>		8
34			3,512			<i>a ≥ c > b</i>		> 50
35		<i>3,508</i>	3,508	vw	w	<i>a > c > b</i>		3
36		3,499	3,500–3,501	vw	3,500	<i>a > c > b</i>		> 10
37			3,492–3,493	3,493	w	<i>a > c ≥ b</i>		> 10
38	3,478	3,480	3,479–(3,483)	3,477–3,479	3,481–3,484	<i>a > c > b</i>		> 100
39			3,473	vw	3,472–3,474	<i>a ≥ c > b</i>		> 10
40			3,467	vw	vw	<i>a > b > c</i>		8
41		<i>3,456</i>	3,456–(3,458)	3,453–3,456	3,456–3,457	<i>a > c > b</i>		> 100
42			3,435w	vw	3,435	<i>c > a > b</i>		5
43		<i>3,428</i>	3,428–3,430	vw	w	a		6
44			3,423–3,424	3,423	vw	<i>a > b > c</i>		3
45		<i>3,420b</i>	–	–	–	–	MW	0
46			vw	w	3,415–3,416	<i>c ≥ a > b</i>		5
47		<i>3,412</i>	3,410–3,412	–	–	a		2
48	3,404	<i>3,406</i>	–	–	–	–		2
49		<i>3,402</i>	3,402	3,400–3,402	vw	<i>a > b > c</i>		5
50			3,399			a		3
51			~3,389vw	vw	vw	<i>a ≈ c > b</i>		23
52					~3,386w	c		1
53			3,379	vw	vw	<i>a > c > b</i>		3
54		<i>3,377</i>	3,377	3,379w	3,378–3,379	<i>c > a > b</i>		5
55			3,374	vw	w	a		2
56			3,368–3,369	vw	3,370–3,373	<i>a > c > b</i>		> 50
57		<i>3,356</i>	3,357–3,358	3,357	3,357	<i>a > b ≥ c</i>	W(?)	23

Table 3 (Contd..)

Band no.	Libowitzky and Beran (1995)	Miller et al.(1987)	ν , cm^{-1}			Pleochroism	NSI	n
			a	b	c			
58					$\sim 3,347\text{vw}$	c		8
59	3,341		3,340vw		3,340vw	$a \approx c > b$		1
60			3,330–3,331	3,331–3,332	3,329–3,333	$a > b > c$		> 50
61		3,328	3,327–3,328	3,327	3,327–3,328	$c > a > b$	W(?)	23
62			$\sim 3,310\text{w}$	$\sim 3,310\text{w}$	$\sim 3,310$	$c > a > b$	W(?)	23
63		3,300	3,298–3,299	3,297–3,299	vw	$a > b > c$		2
64			3,280–3,281	3,281–3,282	vw	$a > b > c$		> 50
65		$\sim 3,260$	3,258–3,260b	vw	$\sim 3,260\text{b}$	$c > a \geq b$	MW	> 10
66			3,240–3,252wb	vw, b	3,229–3,242b	$c > a > b$	MW	> 10
67		3,226	3,222–3,225b	3,222–3,225b	3,222–3,226b	$c > a \geq b$	MW	> 10
68	3,215		3,215vw	3,215vw	3,215vw	$a > b > c$	MW	2
69				vw	$\sim 3,175\text{b}$	$c > b \geq a$	MW	7
70			$\sim 3,168\text{b}$	$\sim 3,168\text{b}$		$a > b > c$	(?)	> 10

saturated olivine. The processes $\text{ILD} \rightarrow \text{CED}$ occur at mantle conditions, whereas the different types of non-intrinsic NSI's are eventually formed at later stages in the history of the host xenolith.

(1) Attempts to discriminate between NSI and [ILD/CED] in the mantle olivines studied

Possible candidates for included “water”-bearing phases, NSI, may be:

- (1.1) Water itself, eventually incorporated in the form of single water molecules, (H_2O) , small clusters, $(\text{H}_2\text{O})_n$ with hydrogen bonds predominantly to the oxygen atoms of the crystalline host matrix, or large clusters of fluid inclusions, $(\text{H}_2\text{O})_{\text{ca.}\infty}$, with hydrogen bonds predominantly between the water molecules themselves.
- (1.2) Serpentine minerals.
- (1.3) Talc.
- (1.4) Amphiboles (e.g. edenite).
- (1.5) Hydrous wadsleyite. One might argue that the lower stability limit of the β -phase is beyond the P, T -range of the present rocks, 19–45 kbar/900–1,450 °C (Sobolev 1974). However, the presence of iron in the system causes the $\alpha \leftrightarrow \beta$ transition to be divariant and to decrease the lower P -stability limit of the β -phase. In addition, the presence of OH^- at the O(1) positions of the wadsleyite structure (Smyth 1987) acts in the same direction. Therefore, hydrous wadsleyite may be a candidate for NIS in olivine.
- (1.6) hydroxyl-bearing members of the humite mineral-group (clinohumite, titanclinohumite, humite, chondrodite, norbergite, phases A and B and super-hydrous phase B).

(1.1) Water:

Spectra of several olivines show very weak features in the low-energy spectra range (Table 3, bands 65 to 69) which

may be assigned to hydrogen-bonded (H_2O) and $(\text{H}_2\text{O})_n$. Their intensity is so low that in Fig. 1, because of the scaling used, only band 67 at $3,225 \text{ cm}^{-1}$ is clearly discernible in $\mathbf{E}||\mathbf{c}$ of samples O-89 and Wt-23/84 (Fig. 1a) and of Ps-92/84 (Fig. 1b). The band at $3,222\text{--}3,224 \text{ cm}^{-1}$ was also observed in olivine from Zabargat (Miller et al. 1987). Figure 2 shows the spectral region with enlarged scales, where the ν_{OH} of respective bands occur. In all spectra of Fig. 2, bands 65 to 69 are clearly polarised, predominantly along c. This indicates that the water molecules, when they give indeed rise to these bands, are orientated with respect to the host matrix. Such an effect is hardly expected for H_2O molecules in the large clusters of fluid inclusions (see above). The energies of the ν_{OH} -vibrations discussed here and tentatively assigned to molecular water, are very low which implies weakening of the O-H bonds by forces acting on oxygen or hydrogen or both. In any case, the usual very broad bands of liquid-like water at around $3,400 \text{ cm}^{-1}$ are not observed. In any case, it seems plausible to treat molecular water here as NIS.

(1.2) Serpentine and (1.3) Talc:

OH^- -valence vibrations in natural serpentine and talc minerals occur in the range $3,710\text{--}3,650 \text{ cm}^{-1}$ (Wilkins and Ito 1967; Farmer 1974; Miller et al. 1987; Fuchs et al. 1998). Unpolarised powder spectra were obtained in such papers.

Figure 1 shows that the polarised spectra of olivines A-176, K-4, Sl-278, X-8 and Tw-48/79 do not display bands in the wave number range mentioned. The same is true for Twd-39 and Sl-98 (Table 1) the spectra of which are not included in Fig. 1. All other olivines of Table 1 show absorptions in the afore mentioned spectral range. Generally, out of the total of 335 olivine crystal grains studied here, 232 do show ν_{OH} -bands in the range $3,710\text{--}3,650 \text{ cm}^{-1}$ where serpentines and talc absorb, the other 103 were free from such OH^- .

Such spectra in the $3,710\text{--}3,650 \text{ cm}^{-1}$ range consist of (i) a broad, complex band system with maximum in the

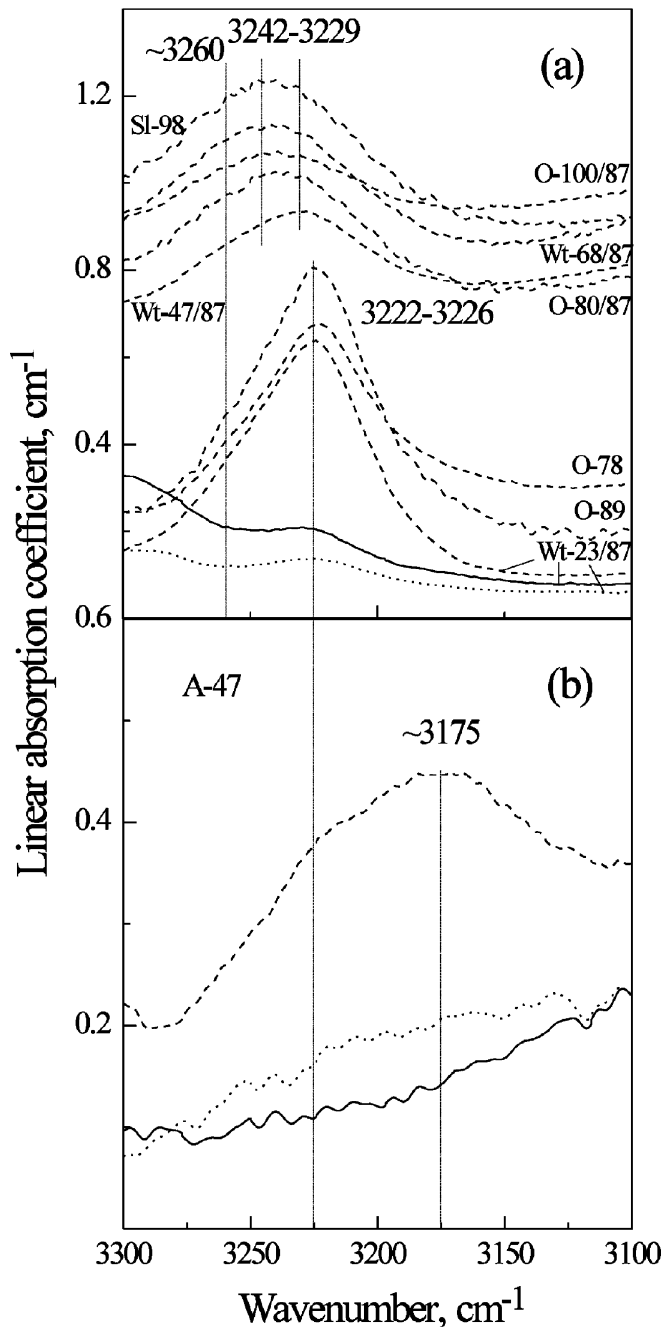


Fig. 2 ν_{OH} -bands below $3,270 \text{ cm}^{-1}$ in some of the olivines studied. These bands are probably to be assigned to valence vibrations of water molecules. Note that these bands are polarised: — ||a,||b, - - - - ||c

range $3,684\text{--}3,692 \text{ cm}^{-1}$, (ii) a sharp band with maximum at $3,677 \text{ cm}^{-1}$ or (iii) both. From Fig. 1 it is obvious that (ii) may occur as the only “water”-bearing phase in the whole spectral range $3,800\text{--}3,000 \text{ cm}^{-1}$, measured (Tw-250/79). In the most often case of (iii), the absolute intensities as well as the intensity ratio of both the maxima may strongly vary (Fig. 1, spectra E||a).

The first mentioned band system (i) is typical of serpentines (Farmer 1974; Miller et al. 1987; Fuchs et al.

1998; own measurements on a ca. $50 \mu\text{m}$ thick vein of pure serpentine, included in Twd-40a/77, cf. Fig. 3), the second one (ii) of Mg-talc (Wilkins and Ito 1967; Miller et al. 1987). The energies of band maxima as well as the half bandwidths are in our spectra the same as those of the respective mineral phases serpentine and talc, themselves. This qualifies the bands as originating from NIS (see above).

From Fig. 1, three remarkable features of the ν_{OH} -bands of talc (ii) and serpentine (i) are obvious:

- (a) In olivine Tw-250/79, talc is the only “water”-bearing phase showing up in the spectra. In this case, ν_{OH} is nearly unpolarised,
- (b) in olivine Tw-9/79, talc and serpentine are the only “water”-bearing phases showing up in the spectra. In this case, the ν_{OH} are strongly polarised along a,
- (c) the spectra of the other olivines of Figs. 1 and 3 to be discussed in a moment, display ν_{OH} of both serpentine (i) plus talc (ii). They show $\nu_{\text{OH(i)(ii)}}$ either almost unpolarised (F-38, Tw-281/79, F-68⁴), or strongly polarised along a (A-379, Ps-92/84, Wt-23/87, O-89, Twd-40a/77, ||b; Twd-29, Ud-118⁴ Wt-47/87, O-80/87, ||a, b). There are also spectra with weak polarisation (Uv-406, F-67 g, A-5, Tw-194/77, F-44⁴).

Observations (a) to (c) indicate that there occur at least two generations of serpentine- and talc-NIS, one orientated with respect to the olivine host structure, the other unorientated. Further, it is remarkable that in the case of cataclastic rock samples from which recrystallised olivines of the ground mass as well as relic olivines could be extracted and studied (Tw-250/79, Tw-48/79 of Table 1), the former contain, if any, traces of serpentine plus talc only, while the relic olivines are always rich in these NIS.

(1.4) Amphiboles:

At higher energies than the wave number range just discussed, $3,710\text{--}3,650 \text{ cm}^{-1}$, there may occur the ν_{OH} maxima of some amphiboles which are typical of metasomatic and metasomatised mantle rocks (Dawson 1980; Ukhanov et al. 1988), namely Mg-edenite with ν_{OH} at $3,711 \text{ cm}^{-1}$ (E||Y,Z), $3,676 \text{ cm}^{-1}$ (E||Y,Z) and $3,653 \text{ cm}^{-1}$ (E||Z) (own measurements on an Mg-edenite from a lherzolite xenolith from Obnazhonnaya) and Mg-pargasite with $3,710$ and $3,678 \text{ cm}^{-1}$ (powder spectra of a synthetic pargasite, Robert et al. 2000).

The superposition of the ν_{OH} -band system of serpentine with the ν_{OH} -bands of talc and amphiboles produces a band system above $3,650 \text{ cm}^{-1}$ which is more complex than indicated by our afore mentioned band maxima $3,692\text{--}3,688$ and $3,677 \text{ cm}^{-1}$.

This is demonstrated by the detailed spectra displayed in Fig. 3, parts (a) to (d). Part (b) of the figure shows strong and broad bands at $3,692\text{--}3,688$ (#3,

⁴Parallelepiped (cf. Table 1)

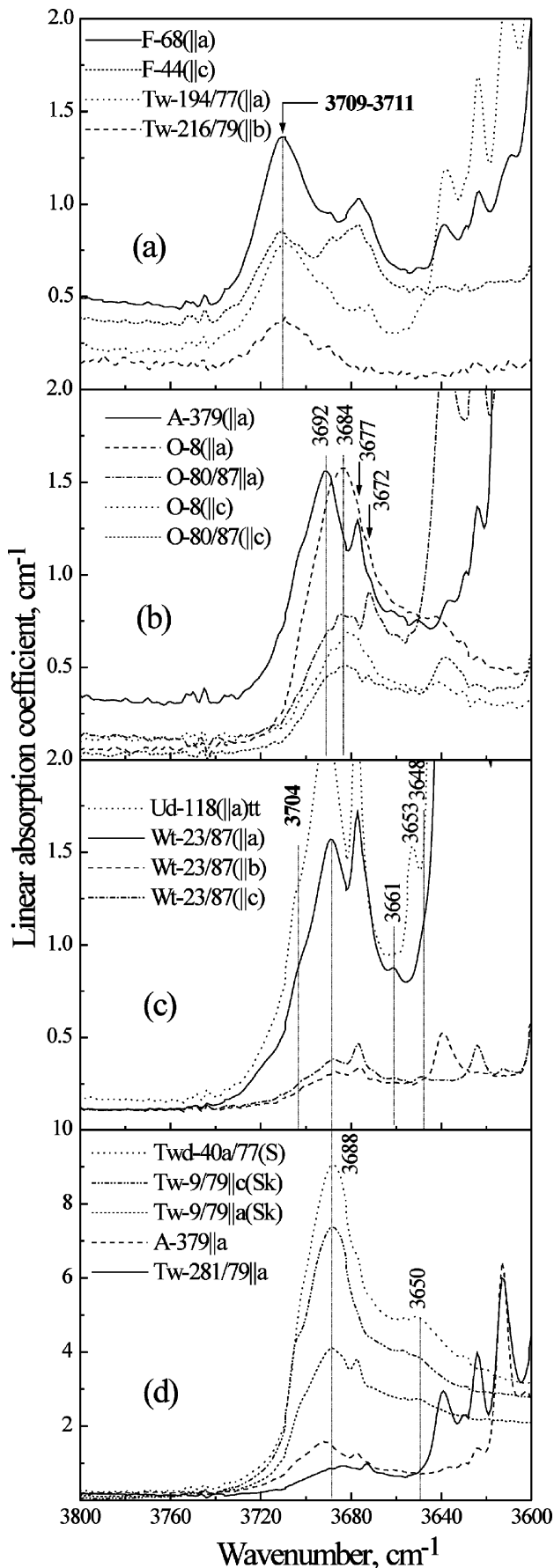


Fig. 3 Some IR-spectra of olivines in the spectral range of the OH^- -vibration of serpentine minerals, some amphiboles and talc. *tt* measurement at 123 °K, S = serpentine in a macroscopic lamellar inclusion

Table 3) cm^{-1} with a shoulder at the high-energy wing, near $3,704 \text{ cm}^{-1}$ (#2). This band system corresponds almost exactly to spectrum *a* of Fig. 5 of Miller et al. (1987), recorded on chrysotile plus lizardite in a KBr-pellet. Thus the band system in our spectra is in accord with that expected for NIS. Other spectra of our olivines display a ν_{OH} -band at $3,684 \text{ cm}^{-1}$ (#4) which corresponds almost exactly to ν_{OH} in lizardite, measured by Fuchs et al. (1998) on a lizardite-*1T* single crystal. Part (d) of Fig. 3 shows also bands #2 and #3 typical of serpentines, eventually #4 as a shoulder. It shows further the weak band at $3,650 \text{ cm}^{-1}$ (#9), which was also observed by Miller et al. (1987) in a chrysotile/lizardite mixture. The ν_{OH} of the NSI just discussed, superimpose in the olivine spectra of Fig. 3, (b) to (d), the ν_{OH} of Mg-talc at $3,677 \text{ cm}^{-1}$ (#5), an energy that is in very good agreement with $3,676.6 \text{ cm}^{-1}$ found by Wilkins and Ito (1967), and with a half bandwidth of 5 cm^{-1} . Such features confirm also talc to occur as NSI in our olivines. In some of the spectra shown in part (d) of Fig. 3, band #5 forms a shoulder only. Characteristically, there occurs a shoulder at $3,672 \text{ cm}^{-1}$ (band #6, see Fig. 1 and Fig. 3(b)) at the low-energy side of the Mg-talc band (#5). This shoulder (#6) forms an own band in some olivines (e.g. O-80/87). Libowitzky and Beran (1995, Table 2) did not differentiate between these two bands #5 at $3,677 \text{ cm}^{-1}$ and #6 at $3,672 \text{ cm}^{-1}$. However, when band intensity correlations to be discussed later, are concerned it is obvious that band #6 correlates, other than #5, with band #30 at $3,535 \text{ cm}^{-1}$. Thus, #6 is really an independent band. It may correspond to ν_{OH} observed for the first time by Sykes et al. (1994) on a boron-containing olivine from Tayozhnoye, Russia. Hence band #6 at $3,672 \text{ cm}^{-1}$ is likely of the [ILD/CED]-type.

(1.5) Hydrous Wadsleyite:

Unpolarised infrared spectra in the ν_{OH} spectral range, $3,800\text{--}3,000 \text{ cm}^{-1}$ measured on randomly oriented, small grains of synthetic hydrous wadsleyite, were presented by McMillan et al. (1991) and by Young et al. (1993). The first mentioned paper assigns a relatively strong band at $3,323 \text{ cm}^{-1}$ to ν_{OH} in wadsleyite, while two other, mostly weaker bands at $3,345$ and $3,404 \text{ cm}^{-1}$ are assigned to hydroxyl in phase B. The spectrum in the second paper displays also the strong ν_{OH} -band of hydrous wadsleyite, nearly at the same energy as in the first paper, $3,329 \text{ cm}^{-1}$, and with a linear absorption coefficient $\alpha_{\text{in}} \approx 300 \text{ cm}^{-1}$ and a full width at half height $\Delta\nu_{1/2} \approx 80 \text{ cm}^{-1}$ (Young et al. 1993; Fig. 6, spectrum *a*). The spectrum just referred to, shows an asymmetry or shoulder at about $3,400 \text{ cm}^{-1}$, on the high-energy wing of

the band at $3,329\text{ cm}^{-1}$. This shoulder is not further commented in that paper. There occur three other, very weak bands at higher energies with wave numbers/linear absorption coefficients as $3,514/20$, $3,580/40$, and $3,615/60$, which the authors interpret also as originating from their hydrous wadsleyite. Kohlstedt et al. (1996) presented unpolarised spectra of hydrous β -phase. These are completely different from the two former ones in that they display a very strong band triplet centred at $3,315\text{ cm}^{-1}$ with components at $3,270$, $3,305$ and $3,380\text{ cm}^{-1}$ with highest $\alpha_{\text{lin}} \approx 500\text{ cm}^{-1}$.

Band #61 at $3,327\text{--}3,328\text{ cm}^{-1}$ in our polarised spectra (Fig. 1) of the olivines A-176 from the diamond-pyrope facies and K-4 from the graphite-pyrope facies, i.e. very high pressure (Table 1), corresponds to the strong ν_{OH^-} -band of hydrous wadsleyite in the two former papers referred to. The polarisation of the band is $c > a > b$ in both olivines, $\alpha_{\text{lin},||c} \approx 2.5$ or 1.9 cm^{-1} and $\Delta\nu_{1/2,||c} \approx 23$ or 19 cm^{-1} in K-4 or A-176, respectively. This band has in $E||c$ a low-energy shoulder at $3,310\text{ cm}^{-1}$, band #62, and an inflection at the high energy wing at $3,357\text{ cm}^{-1}$, band #57. This latter band may correspond to the high-energy shoulder in the spectrum of Young et al. (1993). Figure 1 shows that the polarisation of #57 is $a > b \geq c$, other than that of #61. Thus, it cannot be excluded that bands #61, #62 and #57 in our A-176 and K-4 spectra may be assigned to hydrous wadsleyite. As the half bandwidth in our spectra is even smaller than in the literature spectra, it seems justified to regard hydrous wadsleyite as NSI in our olivines.

At this stage, it should be pointed out, that our spectra do not show the above mentioned bands assigned to phase B (McMillan et al. 1991). On the other hand, our spectra display bands at energies at which the very weak features in the spectra of Young et al. (1993) occur. However, when it comes to the intensity correlations, it will be obvious that these bands do in our spectra not have the same origin as the strong $3,327\text{--}3,328\text{ cm}^{-1}$ “wadsleyite band” #61. Band #61 was observed in olivines O-89 and O-8 (cf. Table 1), which formed in the low-pressure range ($P = 20\text{--}30\text{ kbar}$). Thus, when the assignment of band #61 to hydrous wadsleyite suggested by the above-discussed analogy with spectral results of Miller et al. (1987) and Young et al. (1993), is correct then this phase must be relic in the two olivines from Obnazhonnaya.

(1.6) Hydroxyl-Bearing Humite Minerals, Phases A and B and Superhydrous Phase B:

ν_{OH^-} -bands of the dense hydrous magnesium silicates, phases A and B or superhydrous phase B, are not expected to occur in the spectra of our olivines as such phases require much higher pressures to be stable (Cynn et al. 1996; Kohlstedt et al. 1996) than those of the aforementioned PT -conditions of the olivine host rocks.

Thus, we shall discuss here the possible presence of humite minerals only. These are characterised by the

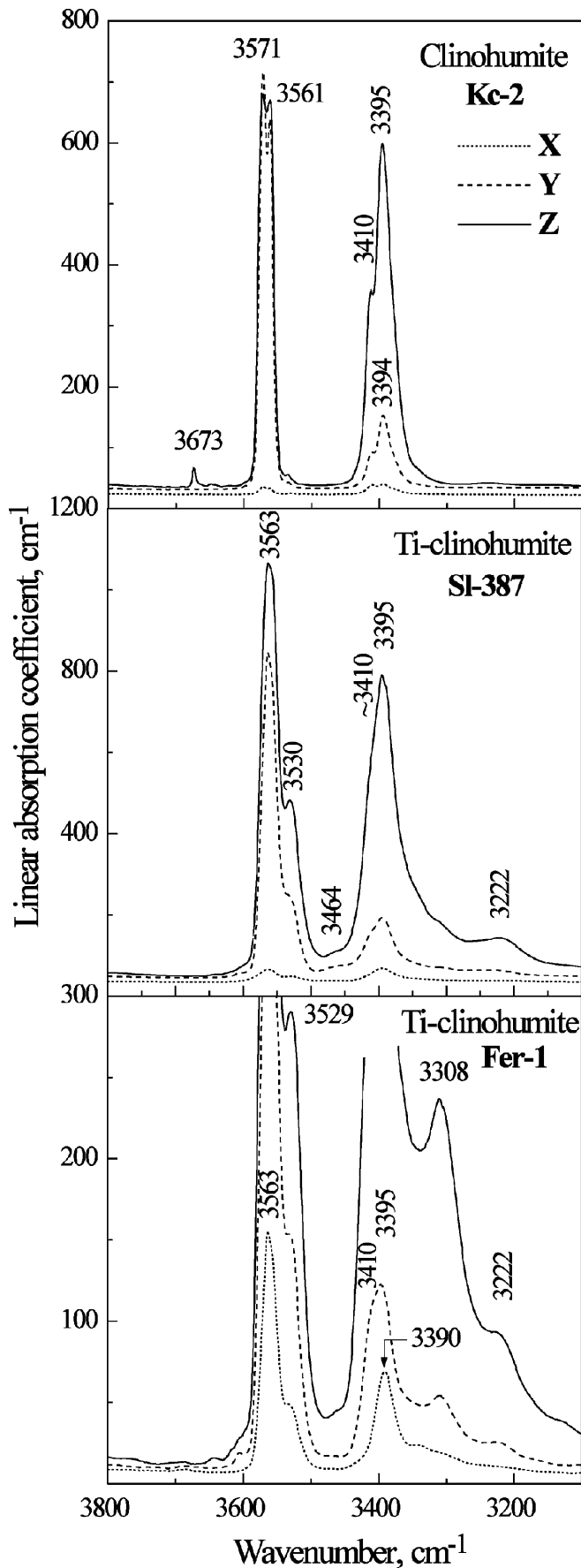
general formula $n \times [\text{M}_2\text{SiO}_4] \times [\text{M}_{1-x}\text{Ti}_x(\text{F},\text{OH})_{2-2x}\text{O}_{2x}]$ with $n=4$ in clinohumite and titanclinohumite, 3 in humite, 2 in chondrodite and 1 in norbergite. M is predominantly Mg, with $\text{Fe}^{2+}/(\text{Fe}^{2+} + \text{Mg})$ fractions usually not higher than 0.1. The crystal structures are closely related to that of olivine (cf. Ribbe 1980).

As reliable polarised single-crystal ν_{OH^-} -spectra are not found in the literature and because the orientation relation between the optical X, Y, Z and the crystallographic a, b, c directions may not be correct due to different choices of the space groups (cf. Jones 1969) of the monoclinic members with $n=4$ and 2 and the orthorhombic members with $n=3$ and 1, we measured such spectra. They are displayed in Figs. 4 and 5. Here, the orientation relations of the orthorhombic members, norbergite and humite, are $X||b$, $Y||c$ and $Z||a$ in accord with space group $Pbnm$, also used in all structure determinations of olivines since Bragg and Brown (1926). The orientation relations for the monoclinic members, clinohumite, titanclinohumite and chondrodite, are $X \perp b$, $Y \perp c$ and $Z||a$ when the crystallographic settings are chosen in accord with space group $P2_1/b$ (cf. Langer et al. 2002). Space groups $Pbnm$ or $P2_1/b$ are used in all structure determinations on humites (cf. Ribbe 1980). Due to the orientation relations just described, the optical directions X, Y and Z of the humites studied here correspond to those of olivine, a presupposition for proving or disproving the presence of humite NSI or CED.

Miller et al. (1987) suggested that ν_{OH^-} -bands in their mantle olivines at $3,572$ and $3,524\text{ cm}^{-1}$, which become the strongest bands in the ν_{OH^-} spectral region on annealing, to be “humite-like OH”. Further, they found in the Zabargat-olivine which, however, is not of mantle origin, bands at $3,572$, $3,525$ and $3,412\text{ cm}^{-1}$ which closely correspond to unpolarised spectra of titanclinohumite (Miller et al. 1987, Fig. 8). Similar conclusions are drawn by Kurosawa et al. (1997, Table 3). Kitamura et al. (1987) proposed that ν_{OH^-} at $3,571$, $3,524$, $3,402$ and possibly $3,319\text{ cm}^{-1}$ in their spectra of an olivine “from a kimberlite” in Buell Park/Arizona, USA, can be assigned to titanclinohumite. These authors discovered planar defects by TEM in their olivine and interpreted them as humite-type layers. The authors described these as made up from OH^- -bearing brucite slabs alternating with olivine slabs in their structure, which is not consistent with the crystal structures of humites (cf. Ribbe 1980; Platonov et al. 2001; Langer et al. 2002 and references therein).

Anyway, the presence of OH^- -bearing titanclinohumite-type be they NSI or CED, in mantle olivines seems to be well established. Chemically, it would result in Si-deficiency of the bulk olivine crystal. This is obvious when we consider that according to the above general formula of humites, their $\text{Si}/(\text{Si} + \text{M})$ -fraction⁵ decreases in the sequence 0.33 in olivine, 0.31 in clinohumite, 0.30

⁵Here, M includes Ti which is extra shown in the above general formula.



in humite, 0.28 in chondrodite to 0.25 in norbergite. Si-depletion of the bulk crystal is also an implication of ILD of the type ($V_{Si} + 4H^+$) (Beran and Putnis 1983; Libowitzky and Beran 1995), which might then be looked at as precursor of humite-like CED and humite NSI in olivine.

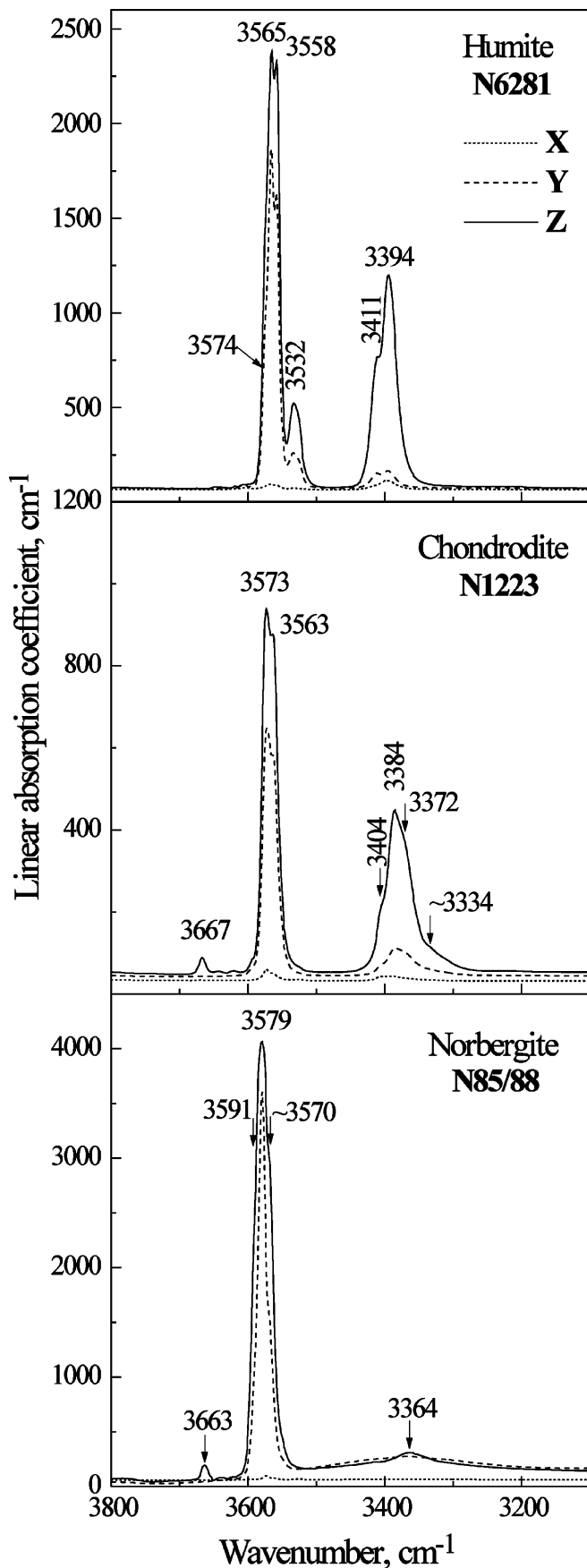
However, Si-depletion is at variance with recent TEM/HRTEM results of Khisina et al. (2001) and Khisina and Wirth (2002): These authors found submicroscopic inclusions, CED, in two mantle olivines most of them forming platelets orientated with respect to the olivine host structure, similar to the observations of Kitamura et al. (1987). EELS analysis proves these CED as depleted in (Mg, Fe^{2+}) rather than in Si as discussed before. This implies that such CEDs are of the Kudoh (2002)-type rather than of the humite-type.

When we now examine the olivine spectra of samples SI-278, X-8, Tw-48/79, Tw-176/79, O-89 and Wt-23/87 in Fig. 1a, we observe bands with energy positions, intensity sequences and polarisations close to those of the bands displayed by the titanclinohumite spectra displayed in Fig. 4. These ν_{OH} -bands are #23 ($3,573\text{ cm}^{-1}$), #26 ($3,562\text{ cm}^{-1}$), #29 ($3,538\text{--}3,541\text{ cm}^{-1}$), #32 ($3,524\text{--}3,525\text{ cm}^{-1}$) and #34 ($3,512\text{ cm}^{-1}$) of Table 3. The intensities, $\alpha_{\text{in}||a}$, of such bands are mutually correlated with each other (see below) such that their relative intensities are independent from their total intensity. This proves the bands to form a “band group” originating from OH^- in the same type of volume element in the olivine structural matrix. Thus, one might conclude that the bands originate from titanclinohumite-NIS in the respective olivines. Indeed the bands under discussion are close to those assigned as “titanclinohumite-like” or as “titanclinohumite bands” in olivines (Miller et al. 1987; Kitamura et al. 1987; Kurosawa et al. 1997). However, the following observations are at variance with an interpretation as NIS:

- (a) ν_{OH} at $3,530\text{ cm}^{-1}$ in titanclinohumite “as a compact mineral” (Fig. 4) splits into bands #29 and #32 in the respective olivines,
- (b) The low-energy components at $3,410$ and $3,395\text{ cm}^{-1}$ typical for all humite minerals except norbergite (Figs. 4 and 5), are missing in the spectra of our above mentioned olivines,
- (c) The bands #23, 26 and #29, 32 show in $E||c$ nearly the same intensity (Fig. 1a: SI-278, X-8, Tw-48/



Fig. 4 Polarised OH-spectra at 298 K of clinohumite and titanclinohumites. The first was extracted from a karbonatite (Ukraine), the second from a mantle Ilm-dunite (cf. Table 1), the last is a titanclinohumite megacryst from the Feruba kimberlite (pipe N1), Guinea, which contains pyrope inclusions (Matsyuk and Kharkiv 1998). The polarised spectra were measured as follows: Kc-2: X(\parallel OAP), Y(\perp AB), Z(\parallel OAP); SI-387: X(\perp AB), Y(\perp OB), Z(\perp OB); Fer-1: X(\parallel OAP), Y(\perp OB), Z(\perp OB). The orientations of the plates are abbreviated as follows: OAP optical axial plane, AB acute bisectrix, OB obtuse bisectrix. For the orientation relations between the axes X, Y and Z of the optical indicatrices and the crystallographic axes (cf. text)



79; and olivine #F-68 in Fig. 6) while in pure titanclinohumite the intensities of the “corresponding” bands differ strongly, $\alpha_{\text{lin}(3563)} \gg \alpha_{\text{lin}(3530)}$ (Fig. 4),

– (d) Spectra of olivine SI-387 (Fig. 1b, Fig. 6) do not show bands #26, 29, 32, 34 despite this olivine is coexisting in the host rock with syngenetic titanclinohumite.

Thus, it is not clear as to whether or not the bands under discussion do really originate from titanclinohumite NIS. Probably “titanclinohumite-like” in the sense of Miller et al. (1987) quoted in the beginning of the section “General considerations”, is a proper term which, in any case, qualifies this band group as originating from CED plus eventually ILD, *i.e.* intrinsic hydroxyl. Hence, we call the bands just discussed, in the following ν_{thl} .

It is remarkable that the olivine spectra displayed in Fig. 1b do not exhibit the ν_{thl} . This becomes obvious when we study the respective parts of the spectra in an enlarged scale. An example is presented in Fig. 6. This figure demonstrates that band #24 ($3,571 \text{ cm}^{-1}$) of SI-387 is not identical with the ν_{thl} -band #23 ($3,573 \text{ cm}^{-1}$) of F-68, because the polarisation behaviour is completely different. Further, low-temperature spectra not shown here, prove that band #24 ($3,571 \text{ cm}^{-1}$) in $\mathbf{E}||\mathbf{c}$ of SI-387 splits to produce bands #23 ($3,573 \text{ cm}^{-1}$) and #25 ($3,566 \text{ cm}^{-1}$), the latter displayed in the RT-spectrum of Twd-24 (Fig. 6).

The intense bands of olivines without ν_{thl} occur all at higher energies up to the minimum at $3,650 \text{ cm}^{-1}$, namely band #10 ($3,639\text{--}3,640 \text{ cm}^{-1}$) to band #22 ($3,575 \text{ cm}^{-1}$), cf. esp. SI-387 and Twd-24 (Fig. 1b). Such bands do not correspond to any OH^- -bearing phase or phases compatible with the chemistry of our olivines (Table 2). This is also true for the distinct low-energy band systems in the range extending from band #64 ($3,280 \text{ cm}^{-1}$) to #36 ($3,500\text{--}3,501 \text{ cm}^{-1}$) showing up in addition to bands #22 to #10, in spectra of A-379, Twd-20, Ps-92/84 and Uv-406 (Fig. 1b), except for bands #62, #61 and #57 (see above). At our best knowledge, one can only conclude so far that these bands are likely to originate from more than one type of OH^- -bearing [ILD/CED] which are so far not identified with respect to their ν_{OH^-} bands. On the other hand, so far no bands or band groups could be assigned to hydroxyl in the (Mg, Fe^{2+})-deficient CED, and their possible ILD precursors, of the type which Khisina and Wirth (2002) discovered in their TEM/HRTEM study and Kudoh (2002) predicted. These observations and considerations strongly suggest that the bands and band groups in the two afore mentioned spectral regions $3,640\text{--}3,575 \text{ cm}^{-1}$ and $3,500\text{--}$

◀

Fig. 5 Polarised OH^- -spectra at 298 °K of humite from Monte Somma, Italy, of chondrodite from Amity, USA, and of norbergite from Pargas Finland. The polarised spectra were measured as follows: N6281: X(\perp AB), Y(\perp OB), Z(\perp OB); N1223: X(\perp AB), Y(\perp AB), Z(\parallel OAP); N85/88: X(\perp AB), Y(\perp OB), Z(\perp OB)

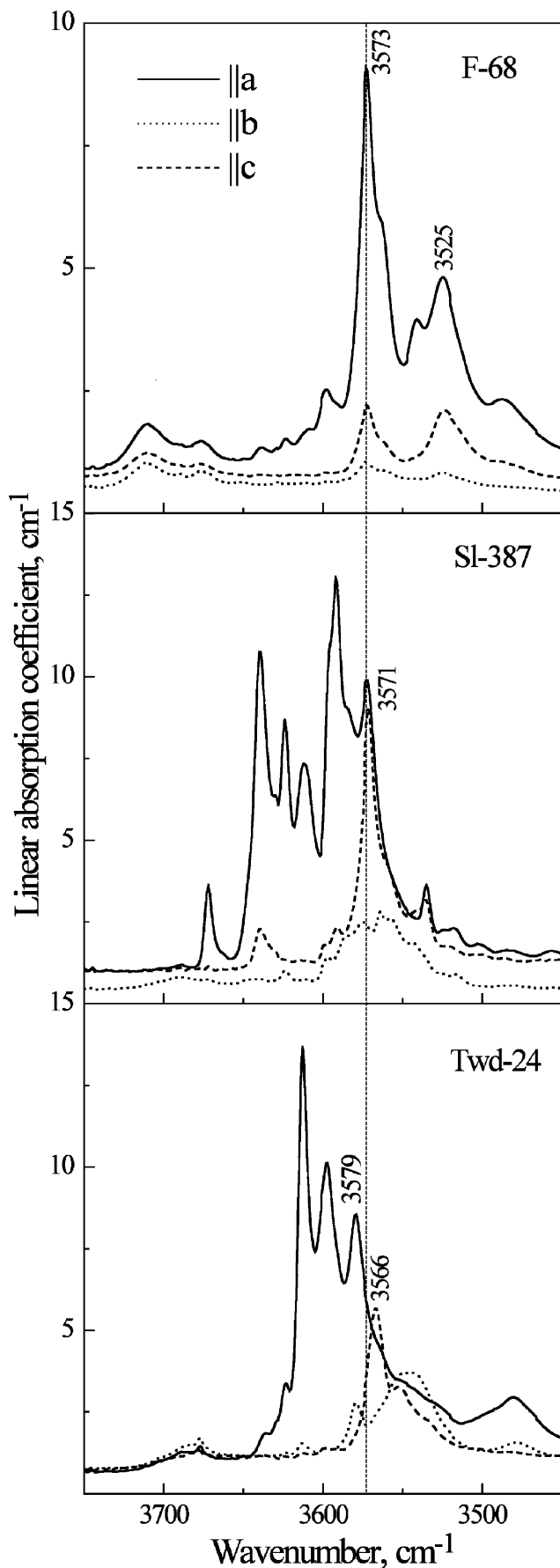


Fig. 6 Enlarged part of the polarised OH⁻-spectra of three olivines showing the complex nature of the OH⁻-bands at around 3,570 cm⁻¹

3,280 cm⁻¹, may be assigned to ν_{OH} in [ILD/CED] of this type. Therefore, we symbolise them as ν_{KWK} in the following, being well aware that the band-assignment indicated by this symbol is still tentative.

(2) Band correlations

The idea behind the attempt to find correlations between intensities of band pairs and/or within supposed band groups is the fact that bands which originate from one specific type of CED and/or NSI will change their intensity in a correlated manner when their concentration in the bulk olivine matrix changes. The presupposition for this is that the chemical nature of the CEDs does not change which might occur in our olivines $\text{Fe}_{0.93-0.84}$ (Table 2).

Figure 7 presents such attempts for the ν_{thl} -group bands #23 (3,573 cm⁻¹), #26 (3,563 cm⁻¹), #29 (3,542 cm⁻¹) and #32 (3,524 cm⁻¹). The intensity in terms of $\alpha_{\text{lin}||\text{a}}$ in cm⁻¹, the linear absorption coefficients of such bands in E||a, are indeed correlated, e.g. #32 with #23 as

$$\alpha_{\text{lin}||\text{a},3524} = -0.027 + 0.397 \times \alpha_{\text{lin}||\text{a},3573}$$

with $r = 0.979$

for $n = 163$ olivines. The slopes of the other correlations in Fig. 7 are approximately the same but the scattering of the data points is larger and consequently, the reliability factors r are somewhat lower. It is remarkable that the r -values are improved when the data of olivines from different rock series (cf. small insert in Fig. 7) are separately fit. Further, correlations $\alpha_{\text{lin}||\text{a},3512} = f(\alpha_{\text{lin}||\text{a},3593,3563,3542,3524})$ confirm that band #34 (3,512 cm⁻¹) is also a member of the ν_{thl} -band group. In this set also, correlation coefficients are improved to $r \geq 0.91$ when data of olivines from different rock series are separately fit.

The reason for such observations may be genetic differences of the olivines from different rock series, which influence the nature of the CEDs. Also, the type of coordination of the OH⁻-dipoles by their next cationic neighbours may be different in the CEDs of olivines from different rock types and series. Without going too far with speculative interpretations, we want to draw here the reader's attention to Fig. 8. From this figure, it is obvious that olivines from different rock series show slightly different $\alpha_{\text{lin}||\text{a},\text{thl}}$ such that olivines from the Mg-series show lower $\alpha_{\text{lin}||\text{a},3563}$ than those of the Mg-Fe-series. In the same direction increases the Fe³⁺-fraction in the olivine M(1) (Fig. 8).

Band intensity correlations in different groups of the ν_{KWK} -bands are already obvious from inspection of the

spectra in Fig. 1b. Examples are displayed in Fig. 9 for one pair in each, the high- and the low-energy ranges of the ν_{KWK} . The correlations are:

$$\alpha_{\text{lin||a},3579} = -0.1834 + 0.4747 \times \alpha_{\text{lin||a},3613}$$

with $r = 0.947$

for $n = 35$ olivines, in Fig. 9a and

$$\alpha_{\text{lin||a},3369} = 0.058 + 0.894 \times \alpha_{\text{lin||a},3331}$$

with $r = 0.989$

for $n = 28$ olivines, in Fig. 9b.

(3) Total intensity, $\sum(\bar{\alpha}_{\text{int}})_{\text{total}}$ yielding total “water”-contents, and intensities of intrinsic hydroxyl of [ILD/CED], $\sum(\bar{\alpha}_{\text{int}})_{\text{[ILD/CED]}}$

Table 4 presents mean total integrated intensities, $\sum(\bar{\alpha}_{\text{int}})_{\text{total}}$, of the ν_{OH} -spectral envelopes as obtained on all the olivine crystal plates of Table 1. We may recall that such data are calculated by summing up mean integrated values $\bar{\alpha}_{\text{int}} = (\alpha_{\text{||a}} + \alpha_{\text{||b}} + \alpha_{\text{||c}})/3$. From the mean total integrated intensities of column 2 in Table 4, we calculate the total “water”-contents listed in column 3 of that Table by means of the equation.

$$c_{\text{wt}\% \text{H}_2\text{O}} = \left(\sum(\bar{\alpha}_{\text{int}})_{\text{total}} \times 1.8 \right) / (\epsilon_{\text{int}} \times D)$$

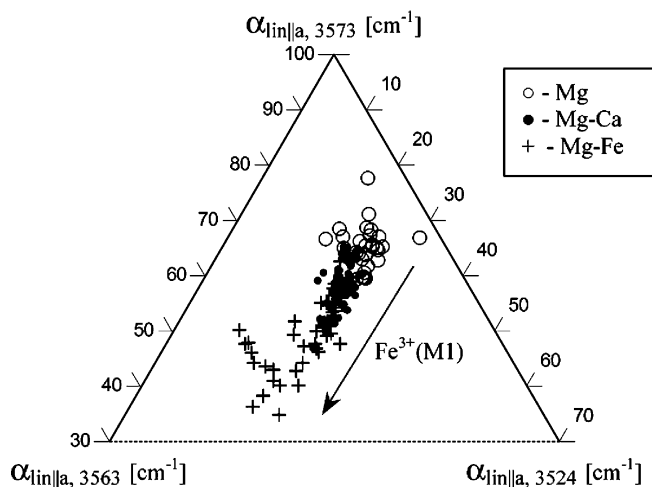


Fig. 8 Relations between intensities, $E_{\text{||a}}$, of three ν_{thl} -bands 3,573(#23), 3,562(#26), 3,525(#32) dependent on the rock series from typical of the olivine host rocks. The $\text{Fe}^{3+}(\text{M1})$ -fraction increases along the *arrow* shown (Matsyuk and Zintchouk 2001)

(Beran et al. 1993) using the mean integrated molar absorptivity $\epsilon_{\text{int}} = 8,812 \text{ [l} \times \text{mole}^{-1}_{\text{H}_2\text{O}} \times \text{cm}^{-2}\text{]}$, obtained from the calibrational data of Bell et al. (2003) by averaging the data on the three olivines studied by these authors, and with the density $D = 3.3 \text{ [g} \times \text{cm}^{-3}\text{]}$ for our olivines.

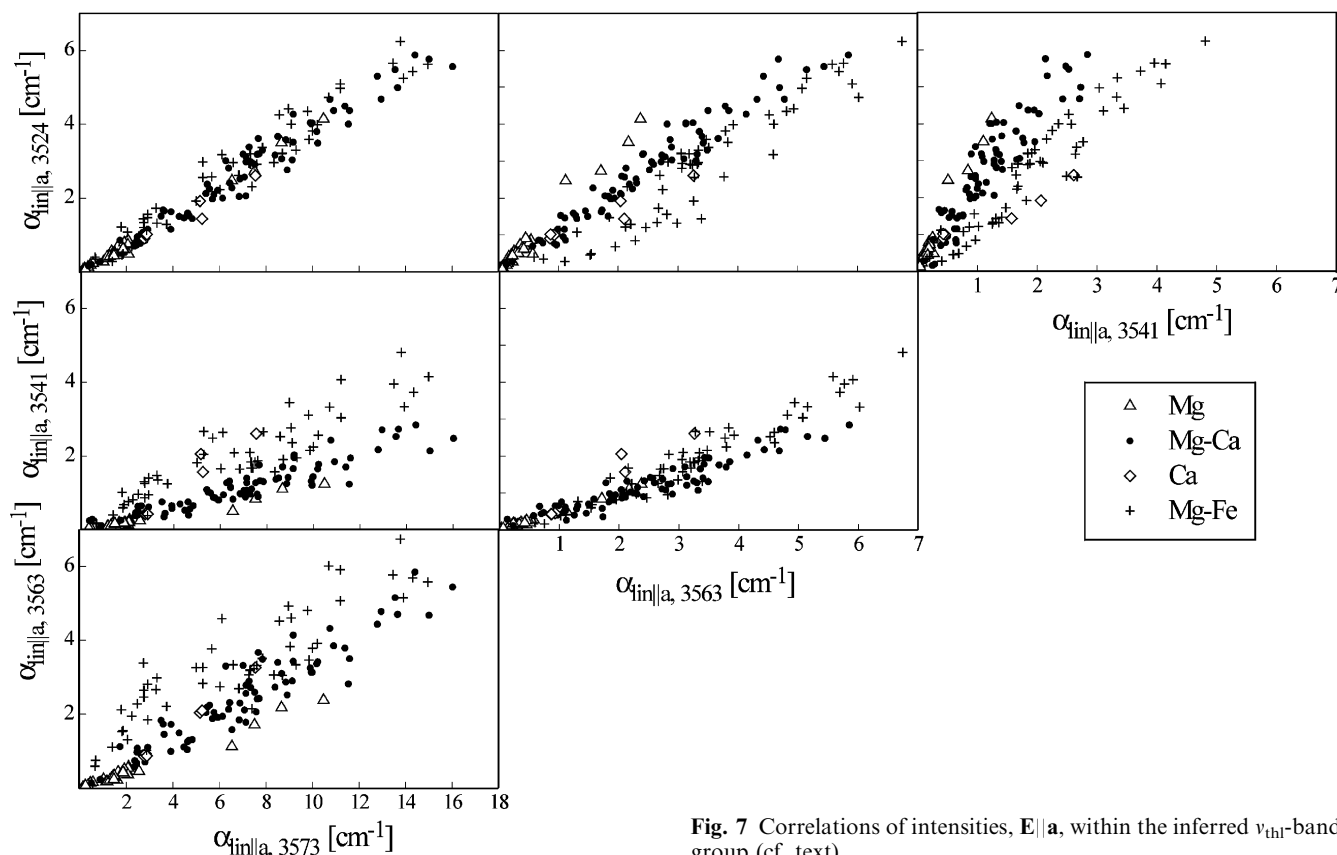


Fig. 7 Correlations of intensities, $E_{\text{||a}}$, within the inferred ν_{thl} -band group (cf. text)

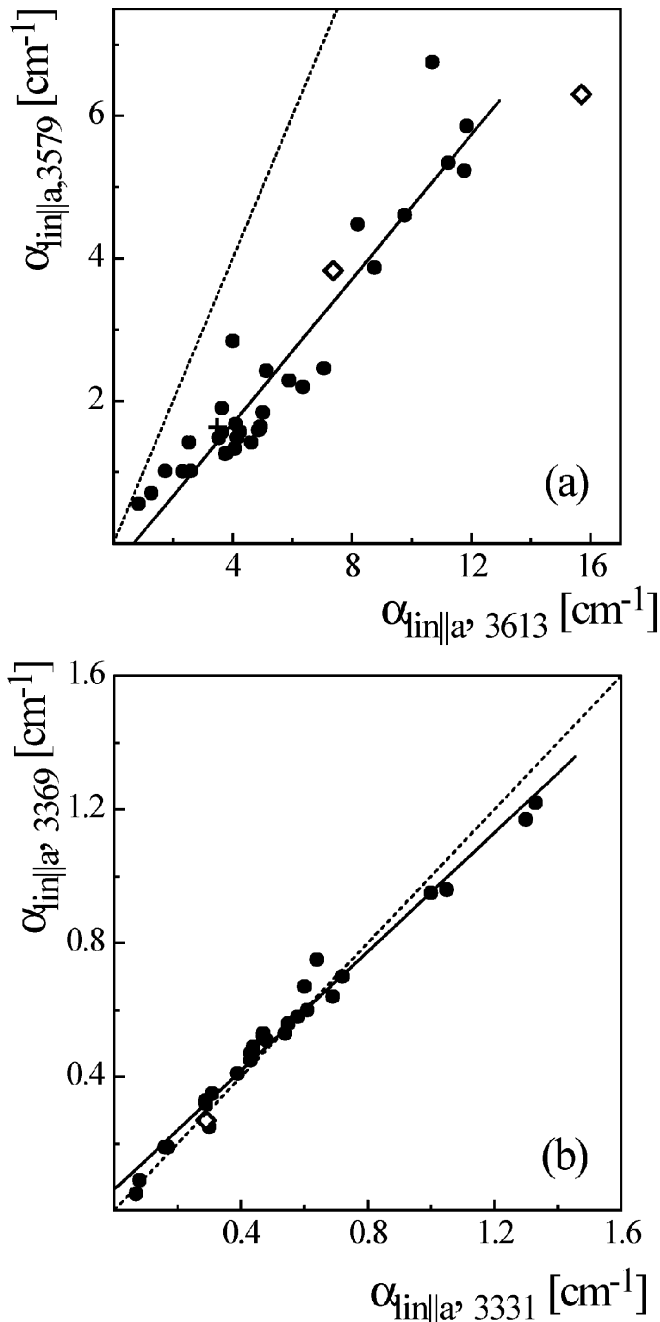


Fig. 9 Examples for intensity correlation of ν_{KWK} -bands of high or low energy (a) or (b), respectively (cf. text). The dotted lines represent a 1:1 correlation. The existing correlation in part (a) deviates strongly from 1:1 because band #14 at $3,613 \text{ cm}^{-1}$ is always more intense than # 21 of $3,579 \text{ cm}^{-1}$

Due to the fact that the ^{15}N NRA-method used by Bell et al. (2003) in the required independent and absolute calibration of ϵ_{int} has an areal resolution of 1 to 2 mm at best (Maldener et al. 2003), this method—as also other macroscopic methods do—averages all the OH^- -bearing species that are present in the volume which is accessible by the method within the olivine crystal grain under study. This means, the quantitative evaluation yields the contents of the structurally

unallocated total “water”, $\text{wt}\% (\text{H}_2\text{O})_{(\text{NSI} + \text{ILD}/\text{CED})}$. Quantitative differentiation between non-intrinsic “water” contents, $\text{wt}\% (\text{H}_2\text{O})_{\text{NSI}}$, and intrinsic “water” contents, $\text{wt}\% (\text{H}_2\text{O})_{[\text{ILD}/\text{CED}]}$, is not possible as the molar absorptivities ϵ_{int} of the structurally different components of the NSI and [ILD/CED] are presumably not the same. However, we may at least calculate $\sum(\bar{\alpha}_{\text{int}})_{[\text{ILD}/\text{CED}]} = \sum(\bar{\alpha}_{\text{int}})_{\text{total}} - \sum(\bar{\alpha}_{\text{int}})_{\text{[NSI]}}$. Such data are listed in columns 4 and 5 of Table 4.

The 34 olivine samples yielding the data in Table 4, were selected from the total of 174 specimens studied, under the view point that all different spectra observed in the whole set be represented. Therefore, several general conclusions can be drawn from the data in Table 4, relating the types of defects and contents of OH^- with the types of olivine occurrences, as e.g. types of their host xenoliths and kimberlites in which these occur:

- (c. 3.1) Olivine included in diamond (C-2/9) does not contain “water”, neither as NSI nor as [ILD/CLD], as far as it can be detected by infrared spectroscopy.
- (c. 3.2) A relation between NIS and [ILD/CED] does not exist. This indicates that NIS may be formed by secondary metasomatic processes, e.g. serpentinisation, *etc.*, within the mantle and/or during uplift of the kimberlitic magma. In fact, different olivine crystals from the same xenolith specimen may or may not contain serpentine- and talc-NIS.
- (c. 3.3) Serpentine plus talc NIS seem to be typical for olivines from rocks from the Mg-Ca-series and to have lowest concentrations in olivines of the Mg-Fe-series.
- (c. 3.4) The two types of talc and/or serpentine NSI, one orientated with respect to the olivine host matrix, (o), the other not, (no), reflect apparently different stages of the above metasomatic processes, (o) an early stage and (no) a late filling of more or less randomly orientated micro-fractures and -cracks in the olivine host crystal.
- (c. 3.5) Amphibole NIS are restricted to olivines from ilmenite-bearing rocks and associations of the Mg-Fe-series.
- (c. 3.6) Not all the olivines of Table 1 are homogeneous with respect of the concentration of “water”-contents or NIS and [ILD/CED]. This is obvious from the ranges of total “water” contents and integrated intensities of NIS and [ILD/CED], quoted in Table 4 for the respective olivines.
- (c. 3.7) Of the rock-forming olivines, those of the ilmenite-bearing specimens are highest in total “water” and [ILD/CED] (samples Tw-194/77, SI-378, SI-98), except for olivines from peridotites with primary phlogopite (e.g. O-106/87, see below).
- (c. 3.8) When relic as well as recrystallised olivines from one and the same xenolith could be studied (Tw-250/79; Tw-48/79 and others), total “water”-contents and [ILD/CED] are found higher to be in the former than in the latter.
- (c. 3.9) Total “water”-contents and [ILD/CED] are exceptionally high in macro- and megacrysts of the Mg-Ca- and Mg-Fe-series. In different types of oli-

Table 4 Total averaged integral ν_{OH} band intensities, $\sum(\bar{\alpha}_{\text{int}})$ [cm^{-2}], and total “water” contents, wt. ppm H_2O , in the olivines studied,

$\bar{\alpha}_{\text{int}} = (\alpha_{\parallel\text{a}} + \alpha_{\parallel\text{b}} + \alpha_{\parallel\text{c}})_{\text{int}}/3$. Types of hydroxyl in olivine: *NSI* non-intrinsic inclusions, *ILD* intrinsic local defects, *CED* clustered extended defects. Columns 4 and 5 split the total $\sum(\bar{\alpha}_{\text{int}})$ into components originating from non-intrinsic “water”-bearing inclusions, $\sum(\bar{\alpha}_{\text{int}})_{\text{NSI}}$, and intrinsic OH^- -bearing defects, $\sum(\bar{\alpha}_{\text{int}})_{\text{CED+ILD}}$ (cf. text). For the calculation of $\bar{\alpha}_{\text{int}}$ from the data obtained by curve analysis of the spectra as well as of wt. ppm H_2O , cf. text. Abbreviations in column 4: *A* amphibole, *MW* molecular water, *S* serpentine, *T* talc, *W* wadsleyite. ^a Different crystal plates of the same orientation yielded spectra with the same shape, but with different intensities. These were averaged to obtain the quoted values. ^b Values measured on parallelepipeds which yielded different $\sum(\bar{\alpha}_{\text{int}})$ in (010) and (001)

Olivine from	$\sum(\bar{\alpha}_{\text{int}})_{\text{total}}$	Total “water” content, wt. ppm H_2O	$\sum(\bar{\alpha}_{\text{int}})_{\text{NSI}}$	$\sum(\bar{\alpha}_{\text{int}})_{\text{CED+ILD}}$
A-176	43.3	27	42.6 (W)	0.7
Tw-176/79	65–69	40–43	6–10 (S, T)	59
Tw-9/79	9	6	9 (S, T, W)	0
A-47	140–144	87–89	77–81 (MW, W, S)	63
O-89	157–168	97–104	11–22 (S, T, W, MW)	146
O-8	65–80	40–50	36 (S, T, MW, W)	29–44 ^a
Ps-92/84	171	106	8 (S, MW)	163
C-2/9	0	0	0	0
Uv-406	174–177	108–110	58–61 (S, T, MW)	116
Tw-40a/77	58–65	36–40	18–25 (S, T)	40
Tw-20	263	163	42 (S, T, MW)	221
Tw-29	94–97	58–60	36–39 (S, T)	58
A-5	311–314	193–194	21–25 (S, T, MW)	290
A-379	271	168	36 (S, T, MW)	235
Tw-250/79(Ol _g)	6–7	3.7–4.3	6–7 (S, T, W)	0
Tw-250/79(Ol _r)	8–10	5–6	8–10 (S, T, W)	0
Tw-281/79	322	199	9 (S)	313
Tw-48/79(Ol _g)	59–172	37–107	0	59–172 ^a
Tw-48/79(Ol _r)	112–309	69–191	0–13 (S, T)	112–296 ^a
Tw-24	422	261	16 (S, T)	407
Wt-23/87	331–352	205–218	54 (S, T, MW)	277–298 ^b
K-4	184	114	84 (W)	100
Ud-118	646–677	400–419	35 (S, T)	611–642 ^b
F-38	566	350	45 (S, T, MW)	520
F-67 g	548	339	57 (S, T, MW)	491
Tw-39	429	266	17 (S, T)	413
Tw-194/77	256–305	159–188	15–18 (A, S, T)	240–287 ^a
Sl-278	293	181	5 (MW)	288
X-8	139	86	0	139
Wt-47/87	339–352	210–218	36 (S, T, MW)	303–315 ^a
Tw-216/79	206–227	126–141	6–7 (A, S)	200–220 ^a
F-44	314	194	20 (A, S, T)	294
F-68	249	154	33 (A, S, T)	217
Sl-98	375	232	28 (S, MW)	346
Sl-387	400–463	248–287	0–7 (S)	393–457 ^a
O-80/87	362–441	224–273	9–36 (S, MW)	353–405 ^a

vines, the total “water”-contents, wt. ppm H_2O , occur in the sequence ground mass crystals < megacrysts < macrocrysts.

- (c. 3.10) In a first approximation, it might appear that in the average the contents of total “water” and [ILD/CED] listed in Table 4 have a tendency to increase in the sequence of the rock series $\text{Mg} < (\text{Mg-Ca}) < (\text{Mg-Fe})$.
- (c. 3.11) Molecular water shows up as weak bands in the spectral range $3,300\text{--}3,100\text{ cm}^{-1}$. These are polarised $\parallel\text{c}$ and occur typically in olivines from xenoliths found in kimberlites from the northern part of the Siberian platform (e.g. Obnazhonnaya; Slyudyanka; cf. Table 1).

(4) Relations between intrinsic ν_{OH} -spectral properties of the olivines and types and origin of their xenolithic mantle host-rocks, as derived from the total of 174 specimens studied, and some petrological implications

The preceding section presented conclusions drawn from the results of the detailed study of the 34 representative specimens in Table 1. In the present section we shall include results of the less fully developed evaluation of

the other 140 olivine specimens. In particular, we shall try to evaluate more broadly the occurrence of the specimens. With this purpose, we come back to Table 3, especially its last column that lists the number of different olivine specimens, n , in which the respective band is observed. In the tentative treatment to be given here, we shall consider—in the first instance—those bands and band groups which occur often in the whole set and occur with more than weak intensities, α_{in} , at least in one of the three polarisations. With these constraints, 29 abundant and strong bands out of the total of 53 bands which we assign to be intrinsic (cf. Table 3) will be discussed. All these 29 bands are strongly polarised along **a**.

The tentative assignment of the major bands and band groups to the types of defects is schematically shown in Fig. 10. Before we use this scheme to discuss the occurrence of the various intrinsic defects deduced above, in relation to the mantle rocks in which the respective olivines occur, we want to point out some general observations and thoughts:

The bands of the Si-depleted [ILD/CED]_(thl) are in almost all cases energetically separated from those of the (Mg,Fe)-depleted [ILD/CED]_(KWK). It is tempting to speculate that this might indicate regimes with different

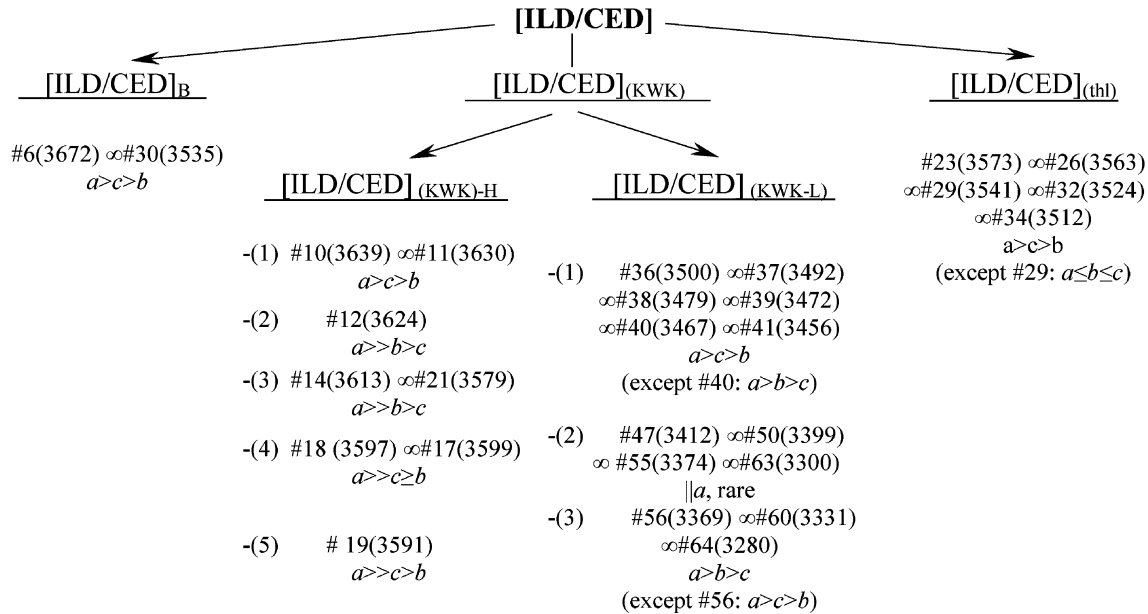


Fig. 10 Types of intrinsic hydroxyl-bearing isolated, local defects, ILD, and condensed, extended defects, CED, inferred in the present study on the basis of the polarised spectra recorded on olivine crystals of 174 specimens of different mantle specimens from the kimberlites of the Siberian platform. Abbreviations: *B* boron-related defect, *thl* titanclinohumite-like defect (Si-depleted), *KWK* Khisina and Wirth (2002) and Kudoh (2002) type defect (Mg-Fe-depleted), *H* or *L* = “high” or “low-energy range” band or band groups, respectively. The band numbers are those of Table 3, the wave numbers in [cm^{-1}] are in parentheses

activity of the SiO_2 -component. If so, $[\text{ILD}/\text{CED}]_{(\text{thl})}$ would be expected to occur in olivines from dunites, while $[\text{ILD}/\text{CED}]_{(\text{KWK})}$ are expected in olivines from pyroxene-bearing rocks like lherzolites and wehrlites. However, such relations are not observed. Contrary, the $[\text{ILD}/\text{CED}]_{(\text{thl})}$ occur typically in the latter rock types. Also, we have to mention that the ν_{OH} of $[\text{ILD}/\text{CED}]_{(\text{KWK})-\text{H}}$ in olivines from some of the wehrlites and harzburgites are energetically not so clearly separated from the (thl)-type defects. If so, the strong band at around $3,570 \text{ cm}^{-1}$, *i.e.* the band which Libowitzky and Beran (1995) call band G, has a complex nature: Band #23 ($3,573 \text{ cm}^{-1}$, $a > c > b$) occurs e.g. in Sl-278 and X-8 (Fig. 1) and forms a group together with band numbers #26, #29, #32, #34, all five being correlated with each other and assigned to the (thl)-type defect (Fig. 10). In the above mentioned olivines from some wehrlites and harzburgites, band #23 contains at least two other bands, #24 and #25 (Table 3), which have slightly different pleochroism than #23.

Considering now the inferred types of intrinsic OH^- -bearing defects (Fig. 10) in relation to the olivines of the whole set of specimens in which they occur, we may distinguish six types:

- (I) Olivines without intrinsic OH^- -bearing defects, at least at the level of the very sensitive IR-absorption spectroscopy with detection limit near 1 wt. ppm “water”. Examples presented in Fig. 1 and Tables 1

and 3, are C-2/9, Tw-250/79, Tw-9/79, A-176. In total, 12 such olivine specimens were found to be of this type. Two are diamond inclusions, the others occur in spinel-dunites and -peridotites of the spinel-pyroxene facies and may indicate very low water fugacity during their formation.

- (II) The boron-related defects $[\text{ILD}/\text{CED}]_{\text{B}}$ occur with intermediate frequency $10 < n < 20$ and are typical for olivines from ilmenite bearing dunite and peridotite xenoliths from Udachnaya and Sludyanka.
- (III) Olivines with only $[\text{ILD}/\text{CED}]_{(\text{thl})}$ as Sl-278 and X-8 (Fig. 1) occur in a total of 10 to 11 specimens, mostly iron-rich ilmenite-peridotites.
- (IV) Olivines with only “high energy” $[\text{ILD}/\text{CED}]_{(\text{KWK})-\text{H}}$, as Sl-387 (Fig. 1) occur typically in harzburgite-dunites from D-Py and G-Py facies. 25 examples were found among the total of 174 specimens. The “low-energy” $[\text{ILD}/\text{CED}]_{(\text{KWK})-\text{L}}$ alone are not found in the whole set of specimens.
- (V) However, “high” and “low-energy” $[\text{ILD}/\text{CED}]_{(\text{KWK})-\text{H}}$ and $[\text{ILD}/\text{CED}]_{(\text{KWK})-\text{L}}$ may occur together, without $[\text{ILD}/\text{CED}]_{(\text{thl})}$ in between the two groups. Spectra of A-379, Tw-20, Ps-92/84 and Uv-406 (Fig. 1) are examples. 30 to 34 other specimens of this type of olivines were found, 12 megacrysts and phenocrysts are among them.
- (VI) Olivines containing “high-energy” and “low-energy” $[\text{ILD}/\text{CED}]_{(\text{KWK})}$ together with $[\text{ILD}/\text{CED}]_{(\text{thl})}$ as F-38 and F-67 g are not rare, ca. 40 such specimens occur in the total set of 174. They are mostly found in cataclastic peridotites, especially in relic olivines as well as in mega- and phenocrysts.

Conclusions

A total of 335 olivine crystal grains were extracted from a set of 174 specimens of Yakutian mantle material. The

set consisted of 97 xenoliths representing all the rock types known from the mantle below the Siberian platform, and 77 mega- or macrocrysts, inclusions in diamonds and in garnet. All olivine grains extracted, were prepared as crystallographically oriented platelets or parallelepipeds, analysed and polarised ν_{OH} -spectra in the range 3,000–3,800 cm^{-1} scanned. Such spectra showed a total of 70 ν_{OH} -bands.

Olivine crystal grains from 34 of the mantle specimens were selected such that all types of spectra observed in the whole set are represented. Careful qualitative and quantitative analysis of these representative spectra and consideration of the relevant literature allowed for distinguishing between OH^- -bands and OH^- -band groups originating either from non-intrinsic, separate inclusions, NSI, or from intrinsic defects which may be either isolated, local, ILD, or condensed, extended defects, CED, in the olivine host structure. As these are likely to be interconnected by intracrystalline condensation reactions and as they cannot be distinguished by IR-spectroscopy, they are summarised and abbreviated as [ILD/CED].

Approximately 53 ν_{OH} -bands of the total of 70 originate from defects intrinsic to the crystal structure of the olivines, 17 originate from nonintrinsic inclusions. Correlations between [ILD/CED] and NSI were not found. This indicates that their geneses are independent. The 29 most abundant, characteristic and intense $\nu_{\text{OH}}[\text{ILD/CED}]$ -bands allow to distinguish between two main types of intrinsic defects: Si-depleted, titanclinohumite-like defects, originally suggested by Miller et al. (1987) and (Mg,Fe)-depleted defects, predicted by Kudoh (2002) and discovered by Khisina and Wirth (2002). We abbreviate these as $[\text{ILD/CED}]_{(\text{thl})}$ and $[\text{ILD/CED}]_{(\text{KWK})}$, respectively. The latter give rise to two different sets, at higher or lower energies compared to the bands of the first defect: $[\text{ILD/CED}]_{(\text{KWK})\text{-H}}$ and $[\text{ILD/CED}]_{(\text{KWK})\text{-L}}$. The three types of defects may occur either alone, as is found for $[\text{ILD/CED}]_{(\text{thl})}$ and the $[\text{ILD/CED}]_{(\text{KWK})\text{-H}}$ or in various combinations as it is depicted in the scheme of Fig. 10.

There exist relations between the occurrence of the intrinsic OH^- and the respective defects in the olivines on the one hand, and the types and genetic peculiarities of their host rocks on the other. However, straightforward and simple relations do not exist. The reasons for this and also for the varieties of intrinsic OH^- -bearing [ILD/CED] may be the following:

- The olivine structure is based on a distorted hexagonally close 2h-oxygen package. This provides the possibility to form a large variety of coherent [CED], based on hexagonally close 2h-arrangement of $(\text{O}_{1-x}\text{OH}_x)$ and formed by intracrystalline condensation of initial, isolated local defects $[\text{V}_{\text{Si}}^{[4]} + 4\text{H}^+]$ as well as $[\text{V}_{(\text{Mg,Fe})}^{[6]} + 2\text{H}^+]$.
- Structural “transition zones” are likely to occur within the rim between the structure of the olivine host and the modified olivine structure of the CEDs.

The potentials in such “transition zones” may differ from those in the olivine host itself and the CED.

- The intrinsic defects reflect the chemistry of the solid as well as of the fluid phase during the olivine formation and all the later events and processes in the mantle and at higher levels.
- Chemical and structural states of the [ILD/CED] may metastably persist under conditions outside the range of their stable existence.
- The nature of the structural defects as isolated ILD and/or condensed CED and the state of the assumed condensation process between them as well as the size of the CEDs may play a role.
- The ILD themselves and their next neighbours may be chemically different such that the potential fields acting on the OH^- -dipoles are different. This will give rise to different band energies.
- Slight chemical and/or structural differences of CED of the same type may give rise to different ν_{OH} .

The most abundant NSI are serpentine plus talc: Of the total of 335 olivine crystals 232 contained such NSI. Two generations of serpentine plus talc NSI could be distinguished, either orientated or unorientated with respect to the olivine host structure. Metasomatic alteration processes, occurring still in the mantle, or during uprising of the kimberlite magma may produce the first or second type of the NSI discussed, respectively.

Mg-edenite and Mg-pargasite occur rarely as NIS alteration products. Hydrous wadsleyite NIS may account for a characteristic, relatively strong band at 3,227–3,228 cm^{-1} with polarisation $c > a > b$ (3,323 cm^{-1} , McMillan et al. 1991; 3,329 cm^{-1} , Young et al. 1993; both unpolarised spectra). We found this NIS in 23 olivines, some from the high pressure D-Py facies, others occur in olivines from rocks formed at relatively low pressure of 20–30 kbar, as e.g. specimen O-89 and O-8 from Obnazhonnaya, where wadsleyite cannot occur except as a relic NIS. Weak bands in the range 3,175–3,260 cm^{-1} which are polarised $c > a > b$, are assigned to hydrogen bonded water molecules occurring as NIS. Humite-minerals were not found as NIS.

We are well aware that further work, especially by TEM/HRTEM-methods is necessary to fully elucidate the role of “water” in mantle olivines.

While the production of the present paper was in the final stage, we learned about the First-Principles study of $[\text{MgH}_2\text{SiO}_4]_x \times n[\text{Mg}_2\text{SiO}_4]$ hydrous olivine Hy-2a with $n=3$ by Churakov et al. (2003), in the— at those days —last issue of Physics and Chemistry of Minerals. We cannot but wish that such theoretical modelling work will in the future contribute to solve the problems of the complex OH^- -valence vibrational spectra of mantle olivines.

Acknowledgements The Yakutian diamond company ALROSA provided the senior author with the authorisation to collect xenolith specimens from the Yakutian kimberlite pipes. N. V. Sobolev, Russian Academy of Sciences, kindly provided olivine grains from Uv-406. I. Krüger, R. T. Schmitt and G. Wappler, Naturkunde-

museum Berlin, provided us with chondrodite and humite samples. S. Herting-Agthe, D. Alscher and Ch. Kotré, Institute of Applied Geosciences, Technical University Berlin, made available samples of norbergite and humite, helped in problems of data processing and manuscript preparation and in XRD-orientation of some of the crystals, respectively. M. Wildner, Geocenter University of Vienna, identified chondrodite 1223 by XRD. F. Galbert (ZELMI, TU Berlin) helped with some electron microprobe analyses. The Deutsche Forschungsgemeinschaft, DFG Bonn-Bad Godesberg, generously provided research stipends every year since 1996 to the senior author. The DFG financed also the FTIR micro-spectrometer used under grant no. La 324/32, as well as other costs of the project. To all these persons and institutions our sincere thanks are due.

References

- Bai Q, Kohlstedt DL (1992) Effects of chemical environment on the solubility and incorporation mechanism for hydrogen in olivine. *Phys Chem Miner* 19:460–471
- Beilby G (1921) *Aggregation and flow of solids*. McMillan & Co, London
- Bell DR, Rossman GR (1992) The distribution of hydroxyl in garnets from the subcontinental mantle of Southern Africa. *Contrib Mineral Petrol* 111:161–178
- Bell DR, Rossman GR, Maldener J, Endisch D, Rauch F (2003) Hydroxide in olivine: a quantitative determination of the absolute amount and calibration of the IR-Spectrum. *J Geophys Res* 108, B2:2105–2113
- Beran A (1969) Über (OH) – Gruppen in Olivin. *Anz Österr Akad Wiss, Math Naturwiss Kl Anzeiger* 73–74
- Beran A, Langer K, Andrut M (1993) Single crystal infrared spectra in the range of OH fundamentals of paragenetic garnet, omphacite and kyanite in an eclogitic mantle xenolith. *Mineral Petrol* 48:257–268
- Beran A, Putnis A (1983) A model of the OH positions in olivine, derived from infrared-spectroscopic investigations. *Phys Chem Miner* 9:57–60
- Bowden F, Hughes TP (1937a) Surface temperature of rubbing solids and the formation of the Beilby-layer. *Nature* 139:152
- Bowden F, Hughes TP (1937b) Physical properties of surfaces. IV. Polishing, surface flow and the formation of the Beilby-layer. *Proc R Soc Lond A* 160:575–587
- Bragg WL, Brown GB (1926) Die Struktur des Olivins. *Z. Kristallogr* 63:538–556
- Churakov SV, Khisina NR, Urusov VS, Wirth R (2003) First-principles study of $(\text{Mg}_2\text{SiO}_4)_n(\text{Mg}_2\text{SiO}_4)_m$ hydrous olivine structures. 1. Crystal structure modeling of hydrous olivine Hy-2a $(\text{Mg}_2\text{SiO}_4)_3(\text{Mg}_2\text{SiO}_4)_m$. *Phys Chem Miner* 30:1–11
- Cynn H, Hofmeister AM, Burnkey PC, Navrotsky A (1996) Thermodynamic properties and hydrogen speciation of dense hydrous magnesium silicates. *Phys Chem Miner* 23:361–376
- Dawson JB (1980) *Kimberlites and their xenoliths*. Springer, Berlin Heidelberg New York, 252 pp
- De Leeuw NH, Parker SC, Catlow CRA, Price GD (2000) Modelling the effect of water on the surface structure and stability of forsterite. *Phys Chem Miner* 27:332–341
- Farmer VC (1974) The layer silicates. In: Farmer VC (ed) *The infrared spectra of minerals*. Mineral Soc Lond Monogr 4:331–363
- Freund F, Oberheuser G (1986) Water dissolved in olivine: a single-crystal infrared study. *J Geophys Res* 91:745–761
- Fuchs Y, Linares J, Mellini M (1998) Mössbauer and infrared spectrometry of lizardite-1T from Fico, Elba. *Phys Chem Miner* 26:111–115
- Jones NW (1969) Crystallographic nomenclature and twinning of the humite minerals. *Am Mineral* 54:309–311
- Kitamura M, Kondoh S, Morimoto N, Miller GA, Rossman GR, Putnis A (1987) Planar OH-bearing defects in mantle olivine. *Nature* 328:143–145
- Khisina NR, Langer K, Andrut M, Uchanov AV, Wirth R (2000) Nano-scale microstructure of Fe^{3+} -, OH^- -bearing crystalline inclusions in experimentally oxidized olivine from a mantle nodule. *Mineral Mag* 64(2):319–335
- Khisina NR, Wirth R, Andrut M, Uchanov AV (2001) Extrinsic and intrinsic mode of hydrogen occurrence in natural olivines: FTIR and TEM investigation. *Phys Chem Miner* 28:291–301
- Khisina NR, Wirth R (2002) Hydrous olivine $(\text{Mg}_{1-y}\text{Fe}^{2+}_y)_{2-x}\text{V}_x\text{SiO}_4\text{H}_{2x}$ – a new DHMS phase of variable composition observed as nanometer-sized precipitations in mantle olivine. *Phys Chem Miner* 29:98–111
- Kohlstedt DL, Kepler H, Rubie DC (1996) Solubility of water in the α , β , and γ phases of $(\text{Mg},\text{Fe})_2\text{SiO}_4$. *Contrib Mineral Petrol* 123:345–357
- Kohlstedt DL, Mackwell SJ (1998) Diffusion of hydrogen and intrinsic point defects in olivine. *Z Phys Chem* 207:147–162
- Kudoh Y (2002) Predicted model for hydrous modified olivine (HyM- α). *Phys Chem Miner* 29:387–395
- Kurosawa M, Yurimoto H, Sueno S (1997) Patterns in the hydrogen and trace element compositions of mantle olivines. *Phys Chem Miner* 24:385–395
- Langer K, Platonov AN, Matsyuk SS, Wildner M (2002) The crystal chemistry of the humite minerals: Fe^{2+} - Ti^{4+} charge transfer and structural allocation of Ti^{4+} in chondrodite and clinohumite. *Eur J Mineral* 14:1027–1032
- Libowitzky E, Beran A (1995) OH Defects in forsterite. *Phys Chem Miner* 22:387–392
- Libowitzky E, Rossman GR (1996) Principles of quantitative absorbance measurements in anisotropic crystals. *Phys Chem Miner* 23:319–32
- Libowitzky E, Rossman GR (1997) An IR absorption calibration for water in minerals. *Am Mineral* 82:1111–1115
- Maldener J, Hösch A, Langer K, Rauch F (2003) Hydrogen in some natural garnets studied by nuclear reaction analysis and vibrational spectroscopy. *Phys Chem Miner* 30:337–344
- Matsyuk SS, Platonov AN, Genschaf YS, Saltikovskiy AJ, Kaminskiy FW, Kepezhinskaya VV (1988) Study of garnets from deep-seated parageneses by optical spectroscopy (in Russian). *Izv Akad Nauk SSSR, Ser Geol* No 7:46–58
- Matsyuk SS, Kharkiv AD (1998) The Paragenesis pyrope + titanclinohumite + clinopyroxene, found for the first time Kimberlites (in Russian). *Doklady RAN* 359, no 3:376–378
- Matsyuk SS, Langer K, Hösch A (1998) Hydroxyl defects in garnets from mantle xenoliths in kimberlites of the Siberian platform. *Contrib Mineral Petrol* 132:163–179
- Matsyuk SS, Zintchouk NN (2001) Optical spectroscopy of the upper mantle minerals (in Russian). Nedra, Moskau, 428 pp
- McMillan PF, Akaogi M, Sato RK, Poe B, Foley J (1991) Hydroxyl groups in β - Mg_2SiO_4 . *Am Mineral* 76:354–360
- Miller GH, Rossman GR, Harlow GE (1987) The natural occurrence of hydroxide in olivine. *Phys Chem Miner* 14:461–472
- Paterson MS (1982) The determination of hydroxyl by infrared absorption in quartz, silicate glasses and similar materials. *Bull Mineral* 105:20–29
- Platonov AN, Matsyuk SS, Khomenko VM, Taran MN, Litvin MA (1988) Absorbing centers as indicators for the evolution of mineral forming matter (in Russian). In: *Teoria mineralogii*. Nedra, Leningrad, pp 79–86
- Platonov AN, Langer K, Wildner M, Polschin EV, Matsyuk SS (2001) The crystal chemistry of the humite minerals: spectroscopic studies and structure refinement of an unusual iron-rich clinohumite. *Z Kristallogr* 216:154–164
- Ribbe PH (1980) The humite series and Mn-analogs. In: Ribbe PH (ed) *Orthosilicates*. *Rev Mineral* 5:231–274
- Robert J-L, Ventura GD, Welch MD, Hawthorne CF (2000) The OH-F substitution in synthetic pargasite at 1.5 kbar, 850 °C. *Am Mineral* 85:926–931
- Smyth RJ (1987) β - Mg_2SiO_4 : A potential host for water in the mantle? *Am Mineral* 72:1051–1055
- Sobolev NV (1974) Deep-seated inclusions in kimberlites and the problem of the composition of the upper mantle (in Russian). *Nauka, Novosibirsk* (264 pp), English translation (1977),

- Brown DA (ed) Boyd FR, Am Geophys Union, Washington, DC
- Sobolev NV, Pochilenko NP, Yephimova ES (1984) Diamond-bearing peridotite xenoliths in kimberlites and the problem of diamond genesis. *Geologiya i geofizika*, N12:63–80
- Sobolev VS, Dobretsov NL Sobolev NV (1972) Classification of deep-seated xenoliths and the type of the upper mantle (in Russian). *Geol Geophys* N12:37–42
- Sykes D, Rossman GR, Veblen DR, Grew ES (1994) Enhanced H and F incorporation in borian olivine. *Am Mineral* 79:904–908
- Tröger WE (1971) *Optische Bestimmung der gesteinsbildenden Minerale*. Teil 1. Stuttgart, 188 pp
- Ukhanov AV, Ryabchikov ID, Kharkiv AD (1988) Lithospheric mantle of the Yakutian kimberlite province (in Russian). Nauka, Moscow, 286 pp
- Wilkins RWT, Ito J (1967) Infrared spectra of some synthetic talcs. *Am Mineral* 52:1649–1661
- Wright K, Catlow CRA (1994) A computer simulation study of OH defects in olivine. *Phys Chem Miner* 20:515–518
- Young TE, Green HW II, Hofmeister AM, Walker D (1993) Infrared spectroscopic investigation of hydroxyl in β -(Mg,Fe)₂-SiO₄ and coexisting olivine: Implications for mantle evolution and dynamics. *Phys Chem Miner* 19:409–422